Received: 4 November 2022 | Revised: 29 April 2023 | Accepted: 26 May 2023

DOI: 10.1096/fj.202201769R

RESEARCH ARTICLE

The FASEB Journal

Cyclin D3 deficiency promotes a slower, more oxidative skeletal muscle phenotype and ameliorates pathophysiology in the *mdx* mouse model of Duchenne muscular dystrophy

Agnese Bonato[1] | **Giada Raparelli**[1] | **Siro Luvisetto**[1] | **Flavia Forconi**[2] | **Marianna Cosentino**[2] | **Felice Tirone**[1] | **Emanuele Rizzuto**[3] | **Maurizia Caruso**[1]

[1]Institute of Biochemistry and Cell Biology, National Research Council, Monterotondo, Italy

[2]DAHFMO-Unit of Histology and Medical Embryology, Sapienza University of Rome, Rome, Italy

[3]Department of Mechanical and Aerospace Engineering, Sapienza University of Rome, Rome, Italy

Correspondence
Maurizia Caruso, CNR-Institute of Biochemistry and Cell Biology, Via Ettore Ramarini 32, Monterotondo 00015, RM, Italy.
Email: maurizia.caruso@cnr.it

Funding information
Duchenne Parent Project, The Netherlands, Grant/Award Number: 19.018; IBSA Foundation for Scientific Research

Abstract

We previously reported that cyclin D3-null mice display a shift toward the slow, oxidative phenotype in skeletal muscle, improved exercise endurance, and increased energy expenditure. Here, we explored the role of cyclin D3 in the physiologic response of skeletal muscle to external stimuli and in a model of muscle degenerative disease. We show that cyclin D3-null mice exhibit a further transition from glycolytic to oxidative muscle fiber type in response to voluntary exercise and an improved response to fasting. Since fast glycolytic fibers are known to be more susceptible to degeneration in Duchenne muscular dystrophy (DMD), we examined the effects of cyclin D3 inactivation on skeletal muscle phenotype in the *mdx* mouse model of DMD. Compared with control *mdx* mice, cyclin D3-deficient *mdx* mice display a higher proportion of slower and more oxidative myofibers, reduced muscle degenerative/regenerative processes, and reduced myofiber size variability, indicating an attenuation of dystrophic histopathology. Furthermore, *mdx* muscles lacking cyclin D3 exhibit reduced fatigability during repeated electrical stimulations. Notably, cyclin D3-null *mdx* mice show enhanced performance during recurrent trials of endurance treadmill exercise, and post-exercise muscle damage results decreased while the regenerative capacity is boosted. In addition, muscles from exercised cyclin D3-deficient *mdx* mice display increased oxidative capacity and increased mRNA expression of genes involved in the regulation of oxidative metabolism and the response to oxidative stress. Altogether, our findings indicate that depletion of cyclin D3 confers

Abbreviations: AMPK, AMP-activated protein kinase; Atrogin-1, alias for F-box protein 32; BSA, bovine serum albumin; CDK4/CDK6, cyclin-dependent kinase 4 and 6; CSA, cross-sectional area; D3, cyclin D3; DMD, Duchenne muscular dystrophy; EDL, extrensor digitorum longus; eMyHC, embryonic myosin heavy chain; GP, gastrocnemius/plantaris; IgG/IgM, immunoglobulin G and M; MEF2, myocyte enhancer factor 2; MHC, myosin heavy chain; MHY3, myosin heavy chain 3 gene; MuRF1, muscle-specific RING finger protein-1; NADH, nicotinamide adenine dinucleotide); NADH-TR, NADH-tetrazolium reductase; NEF2L2/NRF2, nuclear factor erythroid 2-related factor 2; NFAT, nuclear factor of activated T cells; Nfix, nuclear factor I X; PBS, phosphate-buffered saline; PDK4, pyruvate dehydrogenase kinase isozyme 4; PFA, paraformaldehyde; PGC1α, PPAR γ coactivator 1α; PPARδ, peroxisome proliferator-activated receptor δ; SIRT1, silent mating type information regulator 2 homologue 1; SOD 3, superoxide dismutase 3; TA, tibialis anterior; UCP2, uncoupling protein 2; ULK1, Unc-51-like kinase 1; Utrn, utrophin gene.

benefits to dystrophic muscle, suggesting that cyclin D3 inhibition may represent a promising therapeutic strategy against DMD.

KEYWORDS

cyclin D3, Duchenne muscular dystrophy, exercise, *mdx*, oxidative metabolism, skeletal muscle fibers

1 | INTRODUCTION

Duchenne muscular dystrophy (DMD) is an X-linked neuromuscular disease caused by mutations in the gene-encoding dystrophin, a protein essential for muscle fiber membrane integrity. Lack of dystrophin results in high susceptibility of the sarcolemma to contraction-induced injury, leading to a progressive cascade of events, such as inflammation, repeated cycles of degeneration/regeneration, with exhaustion of the muscle progenitor pool, fibrosis, and muscle weakness.[1] These morphological changes are associated with a decrease in oxidative capacity of the muscle, impaired ATP production, and metabolic abnormalities.[2]

Currently, there is no cure for DMD, and its symptomology is treated with glucocorticoids. There are a number of therapeutic interventions that have shown promise in preclinical and early clinical trials, including genetically based therapies that aim at restoring dystrophin expression and molecular and cell-based therapies. Furthermore, therapeutic strategies aiming to protect from degeneration and increase muscle function, by targeting downstream pathological mechanisms, are also being developed to prolong survival, increase quality of life, and improve the effectiveness of pharmacologic and cell-based therapeutic approaches.[3–6]

Skeletal muscle groups consist of heterogeneous and specialized myofibers that differ in their contractile response (slow or fast) and metabolism (oxidative or glycolytic).[7] It has been known for many years that slower, oxidative muscle fibers are more resistant to the dystrophic pathology in comparison with fast, glycolytic fibers both in DMD patients and DMD mouse models.[8,9] Therefore, a proposed therapeutic strategy for treating muscular dystrophy is focused on remodeling skeletal muscle toward a slower, more oxidative phenotype.[10]

Indeed, several works in DMD animal models demonstrate that targeting components of signaling pathways and various transcription factors, coactivators, and corepressors involved in skeletal muscle remodeling can ameliorate dystrophic pathology. For example, activation of the calcium-regulated phosphatase calcineurin in dystrophic muscle results in an increase in proportion of oxidative fibers along with an increase in utrophin A expression and a clear attenuation of the dystrophic phenotype.[11,12] Furthermore, transgenic and/or pharmacologic activation of factors that promote the slow, oxidative phenotype, such as the deacetylase SIRT1, the AMP-activated protein kinase (AMPK), the transcription factor peroxisome proliferator-activated receptor δ (PPARδ), and the transcriptional cofactor PPAR γ coactivator 1α (PGC1α), beneficially alters the phenotype of dystrophic skeletal muscle.[13–16] Likewise, a rescue from the dystrophic pathology was observed in dystrophic mouse models lacking molecules that repress the slow phenotype, such as the transcription factors E2F1 and nuclear factor I X (Nfix).[17,18]

Based on our previous observation that mice lacking cyclin D3 display a shift in skeletal muscle fibers toward the slow, oxidative phenotype,[19] we hypothesized that inactivation of cyclin D3 in the *mdx* mouse model of DMD may beneficially alter the phenotype of dystrophic skeletal muscle.

Cyclin D3 belongs to the family of mitogen-induced D-type cyclins (D1, D2, and D3), the regulatory subunits of the cyclin-dependent kinases CDK4 and CDK6 that drive progression through the G1 phase of the cell cycle by initiating phosphorylation of the retinoblastoma protein.[20,21] Besides retinoblastoma, cyclinD-CDK4/6 complexes target other proteins for phosphorylation,[22] and there is increasing evidence that D-cyclins may also perform kinase-dependent and -independent transcriptional functions and may mediate metabolic responses to external cues even in differentiated non-proliferating cells.[23,24]

D-cyclins are highly homologous, suggesting redundancy in their functions. However, they also perform unique functions, as indicated by different substrate specificity, different tissue-specific expression patterns, and different phenotypic consequences of cyclin D knockouts in mice.[22,25–29]

In skeletal muscle, cyclin D3 is expressed at high levels during the late stages of fetal development and early postnatal life,[30] and during adult regenerative myogenesis.[31] Also, expression of cyclin D3 mRNA is increased in *mdx* muscle.[32]

We previously demonstrated that cyclin D3 plays a unique function in controlling the proliferation/differentiation balance of myogenic progenitor cells, and the proper timing of muscle regeneration upon acute muscle injury.[31] In addition, we described a role of cyclin D3 in

the regulation of muscle and whole body metabolism.[19] In particular, we showed that mice lacking cyclin D3 display a switch toward a slower, more oxidative myogenic program, accompanied by enhanced exercise capacity and increased energy expenditure.

In the current study, we further explored the role of cyclin D3 in muscle physiology by analyzing the response of cyclin D3 null mice to external stimuli. In addition, we generated and analyzed dystrophic mice lacking cyclin D3 to verify whether the muscle phenotype observed in cyclin D3- null mice would alleviate DMD pathogenesis.

2 | MATERIALS AND METHODS

2.1 | Mice

Cyclin D3 knockout mice ($D3^{-/-}$) were generated along with $D3^{+/+}$ controls by interbreeding $D3^{+/-}$ heterozygous animals kindly provided by Piotr Sicinski (Dana Farber Cancer Institute, Boston MA). *mdx* mice (C57BL/10ScSn-Dmd^{mdx}/J) were purchased from Charles River, Italy. $mdx/D3^{-/-}$ double-mutant mice were generated through three subsequent crossings. The F0 was obtained by crossing *mdx* female and $D3^{+/-}$ male mice. The F1 generation was initiated by crossing $mdx/D3^{+/-}$ males from the F0 generation and *mdx* females. Female and male $mdx/D3^{+/-}$ mice from the F1 generation were then intercrossed to initiate the colony that generated the $mdx/D3^{+/+}$ and $mdx/D3^{-/-}$ progeny used in this study.

Genotyping was performed by PCR using genomic DNA from tail tips as previously described.[28] Animals were maintained in standard cages under a 12:12 light/dark cycle, with light on at 07:00 a.m. Room temperature ranged from 21 to 24°C and humidity was kept constant (55 ± 10%). Food and water were available ad libitum.

Animal procedures were performed on male and female mice and completed in accordance with the European Union Council Directive of September 22, 2010 (2010/63/EU) and the experimental protocol approved by the Italian Ministry of Health (Authorizations n° 269/2019-PR and n° 529/2021-PR).

2.2 | Food starvation and voluntary wheel running

Food deprivation and voluntary wheel running studies were performed using 5- to 6-month-old $D3^{+/+}$ and $D3^{-/-}$ mice. For starvation, animals were subjected to 24 h of food deprivation with ad libitum access to water. For voluntary wheel running exercise, mice were housed for 17 days in cages equipped with wheel carrying automatic counters to monitor the running distance. Mice were sacrificed within 1 h after the end of the experimental procedures.

2.3 | Treadmill running

Exercise studies were performed on a five-lane motorized treadmill equipped with an electronic control unit (Treadmill Model LE8710, PanLab, Comella, Barcelona, Spain) and an electric shock grid at one end of the treadmill. Shock intensity was set at 0.2 mA. The inclination of the treadmill was set at 0°. Mice were familiarized with the treadmill apparatus for 2 min before starting the belt followed by a running with speed set at 6 m/min. Each mouse was immediately removed from treadmill after three electric shocks. One day after habituation, mice were subjected to an endurance protocol, repeated once a week for 5 consecutive weeks, with belt running at accelerated speed. Mice were first acclimated with treadmill for 2 min, followed by a running session with belt speed initially set at 12 m/min. At 5 min after the initiation of exercise, the speed was increased by 1 m/min every 2 min and exercise continued until exhaustion.[33]

2.4 | Force measurements

2.4.1 | In-situ force measurements

Force measurements were performed on tibialis anterior (TA) muscle through the in-situ methodology, by stimulating the TA through the sciatic nerve.[34,35] Mice were anesthetized with an intraperitoneal injection of ketamine chlorhydrate (Ketalar). The distal tendon of the TA was cut a few millimeters far from the end of the muscle, and surrounding muscles were removed to expose the sciatic nerve. The TA tendon was connected to the level arm of a dual-mode 305C-LR actuator/transducer system (Aurora Scientific, Aurora, ON, CA). Muscle contractility was elicited by stimulating the sciatic nerve with a pair of wire electrodes. Square-wave electrical pulses of about 7 mA with a duration of 1 ms were generated by a pulse stimulator (701C, Aurora Scientific). For each experiment, the initial muscle length was adjusted to the optimal length (L_0), which produced the highest twitch force,[34] and muscle cross-sectional area (CSA) was estimated as previously reported.[35,36]

2.4.2 | Measurement protocol

Twitch force and contractile kinetics parameters [time to peak (TTP), half relaxation time (1/2RT), and maximum

value of force derivative (dF/dt)] were measured by stimulating the muscle with a single pulse. After that, the TA muscle was subjected to repeated eccentric stimulations to evaluate the force drop as the measurement of muscle susceptibility to contraction-induced injury.[37] The muscle was stimulated with eight 500 ms pulse trains at the tetanic frequency of 120 Hz with a resting period of 150 s before each of them.[38] After 300 ms of stimulation, the muscle was lengthened by 10% of its L_0, for the remaining 200 ms. The isometric force generated by the specimen during each contraction was recorded and the force drop was computed as the value of the force developed during each eccentric stimulation divided by force developed during the first stimulation.

2.5 | Cryosections, histology, and immunostaining

Freshly dissected extensor digitorum longus (EDL), gastrocnemius–plantaris (GP), and TA muscles were embedded in Tissue Tek O.C.T. compound (Sakura Finetek, Torrence, CA, USA*mdx*, snap frozen in liquid nitrogen-cooled isopentane, sectioned with 8 μm thickness on a cryostat (Leica CM1850UV), and mounted onto poly-L-lysine-coated glass slides.

Hematoxylin and eosin staining was performed on muscle sections fixed with 4% paraformaldehyde (PFA). Sections were stained with Mayer's hemalum solution (cat# T865) and then with Eosin Y solution (cat# X883) following the manufacturer's instructions (ROTH GmBH, Karlsruhe, DE). Slides were rinsed with distilled water, dehydrated in ethanol, cleared with xylene, and mounted with EUKITT (cat# 03989, Sigma-Aldrich, Merck KGaA, Darmstadt, Germany).

Nicotinamide adenine dinucleotide (NADH) dehydrogenase activity was determined by incubating unfixed muscle sections with 0.4 mg/mL NADH disodium salt and 0.8 mg/mL 4-nitro blue tetrazolium chloride (cat# 10107735001 and 11 383 231 001, Roche Diagnostics Basel, CH) in 0.1M Tris–HCl (pH 7.5). Sections were then subjected to sequential dehydration in 80%, 90%, and 100% ethanol, cleared with xylene, and mounted with EUKITT.

Sirius red staining was used to detect extracellular matrix deposition and fibrosis. Briefly, muscle cryosections were thawed and then fixed with Bouin's solution (cat# HT10132, Sigma-Aldrich) for 60 min, washed, and then stained with pricosirius red dye (Direct Red 80, cat# 365548, Sigma-Aldrich) for 60 min. Sections were then sequentially dehydrated in 90% and 100% ethanol, cleared with xylene, and mounted with EUKITT.

Adult and embryonal myosin heavy-chain (MHC) immunostaining was performed on serial 8-μm-thick, unfixed transverse muscle sections. Sections were permeabilized with 0.4% Triton X-100 in phosphate-buffered saline (PBS) buffer for 10 min and incubated in block solution (3% goat serum or 1.5% + 1.5% goat and donkey serum in PBS) for 60 min, at room temperature (RT). Immunostaining for the F4/80 pan-macrophage surface marker was performed on sections fixed with cold acetone and blocked with 4% bovine serum albumin (BSA) in PBS for 60 min at RT. Primary antibodies were diluted in block solution and applied overnight at 4°C. After two washes in PBS, sections were incubated with the appropriate secondary antibodies, diluted in block solution, for 60 min at RT, and then washed twice in PBS. The nuclei were counterstained by 5 min incubation with Hoechst 33258 (Sigma Aldrich; 1 mg/mL in PBS) and slides were then washed with PBS and mounted with glycerol diluted in PBS (3:1). The slides immunostained for MHCs were post-fixed with PFA (4% in PBS) for 10 min before mounting. For MHC detection, the following primary monoclonal antibodies were used as tissue culture supernatants: SC-71 (MHC-2A, 1:5), 6H1 (MHC-2X, 1:10), and F1.652 (embryonal MHC, 1:20). These antibodies were from DSHB (Developmental Studies Hybridoma Bank, at the University of Iowa, USA). Macrophages were detected with rat anti-mouse F4/80 monoclonal antibody (cat# MCA497G, Bio-Rad Laboratories, Hercules, CA, USA). Laminin was detected with anti-laminin rabbit polyclonal antibody (cat# L9393, Sigma-Aldrich). The secondary antibodies were as follows: goat anti-rabbit Alexa-fluor 488 (cat# A11034) and goat anti-mouse Alexa-fluor 594 (cat# A11032) purchased from Thermo Fisher (Waltham, MA, USA); donkey anti-rat TRITC (cat# 712-025-150), donkey anti-mouse IgM Cy3 (cat# 133178), goat anti-mouse IgG1 Biotin-SP-conjugate (cat# 115-065-205), and Streptavidin Alexa-fluor 488-conjugate (cat# 016-540-084) purchased from Jackson ImmunoResearch (West Grove, PA, USA).

For detection of necrotic fibers, sections were fixed with 4% PFA for 10 min. After three washes in PBS, sections were blocked for 60 min at RT with a solution containing 4% IgG-free BSA (cat# 001-000-161, Jackson ImmunoResearch) in PBS. Anti-laminin primary antibody (cat# L9393, Sigma-Aldrich) and biotinylated anti-mouse IgG and IgM antibodies (cat# 115-065-068, Jackson ImmunoResearch) were diluted in block solution and applied for 2 h at RT. After two washes with 2% IgG-free BSA in PBS, sections were incubated for 60 min at RT with goat anti-rabbit Alexa-fluor 488 secondary antibody (cat# A11034, Thermo Fisher) and Streptavidin Alexa-fluor Cy3-conjugate (cat# 016-160-084, Jackson ImmunoResearch), diluted in block solution. After two washes in PBS, the nuclei were stained for 5 min with Hoechst 33258 and then mounted with glycerol diluted in PBS (3:1).

Images were acquired with an epifluorescence Olympus BX53 microscope equipped with a RLT3 camera,

or a Leica Microdissector LMD7000 equipped with a Leica DFC345 FX camera, controlled by Leica Application Suite X (LAS X). Reconstructed sections were obtained from overlapping individual images assembled with the Adobe Photoshop software or directly by the mosaic function of LAS X software.

Quantifications of histological and immunofluorescence data were performed using ImageJ software version 1.52e, (https://imagej.nih.gov/ij/download.html). For assessment of muscle fiber size, about 80% of total fibers within each muscle cross-section were manually outlined, and the cross-sectional size of each fiber was determined using two different geometrical parameters: the "area" and the minimal "Feret's diameter" (i.e., the minimum distance of parallel tangents at opposing borders of the muscle fiber). The variability of fiber size was obtained by calculating the variance coefficient of the muscle fiber size, defined as follows: variance coefficient = (standard deviation of the muscle fiber size/mean muscle fiber size) x1000.[39] Fibrosis was assessed by measuring the Sirius red-positive areas in entire muscle cross-sections using the SiriusProfiler pipeline built with CellProfiler software (www.cellprofiler.org).[40]

2.6 | Protein extraction and Western blotting

Total TA and GP muscles were homogenized in a modified RIPA lysis buffer (50 mM Tris–HCl pH 7.5, 150 mM NaCl, 2 mM EDTA, 1% Triton X-100, 0.25% sodium deoxycholate, 0.1% SDS, and 10% glycerol) supplemented with protease and phosphatase inhibitors (aprotinin, leupeptin, and pepstatin, 5 μg/mL each; beta-glycerolphosphate, 5 mM; sodium-ortovanadate, 1 mM; sodium fluoride, 10 mM; and phenylmethylsulfonyl fluoride, 1 mM). Samples were sonicated two times at 50 pulses for 10 s, incubated at 4°C for 20 min with agitation, and then centrifuged at 12 500 *g* for 20 min at 4°C to pellet insoluble material. Supernatants were assayed for protein concentration using a conventional Bradford protein assay. For detection of utrophin, TA muscles were homogenized in denaturing lysis buffer (62.5 mM Tris–HCl pH 6.8, 2% SDS, 5 mM EDTA, and 10% glycerol), samples were heated at 50°C for 20 min, mixed and reheated for 5 min, and then centrifuged. Protein concentration was determined using a BCA protein assay kit (cat#71285, Merck Millipore, Burlington, MA, USA). Muscle homogenates (30–40 μg) were separated by sodium dodecyl sulphate–polyacrylamide gel electrophoresis and transferred overnight on nitrocellulose membrane (cat# GE10600002, Sigma Aldrich) for Western blotting. Equal protein loading and transfer were verified by Ponceau S staining. Filters were blocked for 60 min at RT in Tris-buffered saline, 0.1% Tween20 Detergent (TBST) + 5% non-fat milk (NFM), and then incubated overnight at 4°C with primary antibodies (diluted in TBST +5% BSA). After three washes in TBST, filters were incubated for 60 min at RT with peroxidase-conjugated secondary antibodies (diluted in TBST +2.5% NFM).

The primary antibodies used were as follows: anti-AMPKα and anti-phospho-AMPKα (Thr172) rabbit mAbs (cat# 2532 and cat# 2535) obtained from Cell Signaling Technology, Danvers, MA, USA; anti-α-tubulin and anti-vinculin mouse mAbs (cat# T9026 and cat# CP74) obtained from Sigma-Aldrich, Merck; anti-PGC1α and anti-NRF2 rabbit polyclonal antibodies (cat# A12348 and cat# A1244) obtained from ABclonal, Dusseldorf, Germany; and anti-utrophin mouse mAb (cat# 610896, BD Biosciences, Franklin Lakes, NJ USA). The secondary antibodies were as follows: peroxidase-conjugated donkey anti-rabbit (cat#: 711-035-152) and donkey anti-mouse (cat#: 715-035-150) obtained from Jackson InnunoResearch.

Proteins were revealed using the Immobilon western chemiluminescent HRP substrate (cat# WBKLS0500, Merck Millipore). Chemiluminescence was detected by the ChemiDoc XRS+ Gel Imaging System, controlled by Image Lab image capture and analysis software (Bio-Rad, Hercules, CA, USA).

2.7 | RNA isolation, reverse transcription, and real-time PCR

Total RNA was extracted from homogenized muscle tissue using the Trizol reagent (cat# 15596018, Thermo Fisher) according to the manufacturer's instructions. The RNA was treated with RQ1 RNAse-free DNAse (cat# M6101) and retrotranscribed using random hexamer primers (cat# C1181) and MMLV reverse transcriptase (cat# M1705), all obtained from Promega (Madison, WI, USA). Gene-specific primer pairs were designed with the Beacon Designer software (PREMIER Biosoft, San Francisco, CA, USA) or the PrimerBlast resource (https://www.ncbi.nlm.nih.gov/tools/primer-blast/). Amplification was carried out using the SYBR Select Master Mix (cat# 4472919) obtained from Thermo Fisher and an ABI7900HT Fast Real-Time PCR System (Applied Biosystems, Thermo Fisher). Identity of the amplicons was verified by their dissociation curves. The mRNA expression values were normalized to those of the TATA-binding protein gene (TBP) used as endogenous control. All values were obtained in triplicate and the analysis of output values was made using standard ΔΔCt method.

Gene-specific primer sets used for real-time PCR were as follows.

Gene	Accession Number	Forward primer	Reverse primer
Tbp	NM_013684	CCAATGACTCCTATGACCCCTA	CAGCCAAGATTCACGGTAGAT
cyclinD1	NM_007631	GAGATTGTGCCATCCATGC	CTCCTCTTCGCACTTCTGCT
cyclinD3	NM_007632	GGAAGATGCTGGCATACTGG	CCAGGTAGTTCATAGCCAGAGG
Myogenin	NM_031189	CATCACGGTGGAGGATAT	AGCCTGACAGACAATCTC
MYH3	NM_001099635	CAATAAACTGCGGGCAAAGAC	CTTGCTCACTCCTCGCTTTCA
SOD3	NM_011435	GGCCTTCTTGTTCTACGGCT	GCTAGGTCGAAGCTGGACTC
NEF2L2	NM_010902	CTACAGTCCCAGCAGGACAT	TCAAACACTTCTCGACTTACTCCA
PPARδ	NM_011145	CATGGGACTCACTCAGAG	AGATGGACTGCCTTTACC
PDK4	NM_013743	AGCTGCTGGACTTTGGTTCA	CGGTCAGGCAGGATGTCAAT
UCP2	NM_011671	AAGCAGCCTCCAGAACTC	GACCTTCAATCGGCAAGAC
PGC1α	NM_008904	CGGTCTTAGCACTCAGAA	AATTCTCGGTCTTAACAATGG
ULK1	NM_009469	TTACCAGCGCATCGAGCA	TGGGGAGAAGGTGTGTAGGG
Atrogin1	NM_026346	TGAGCGACCTCAGCAGTTAC	TTCTCTTCTTGGCTGCGACG
MuRF1	NM_001039048	ACCACAGAGGGTAAAGAAGAACA	GCAGAGAGAAGACACACTTCCC
Utrn	NM_011682	AGCCTTTGGATTATACTGAAACTCA	CTGTACATCATTGTGTTCATCAGA

2.8 | Statistical analyses

All data are reported in dot plots or in histograms as mean ± standard error of the mean (SEM). The number of animals or samples for each experiment is indicated in the figure legends.

Homogeneity of variances across experimental groups was assessed by Bartlett's test. Data comparisons between two groups were made using two-tailed unpaired Student's *t*-test or Mann–Whitney U-test, as appropriate. Comparisons between three or more groups were assessed by one-way ANOVA, when considering only one independent variable, or by two-way ANOVA when considering the effect of two factors on a dependent variable. Two-way ANCOVA was used to analyze running time including body weight as covariate in the treadmill running experiments. Two-way repeated-measures ANOVA was used to analyze the drop in muscle force produced across repetitive stimulations. Post hoc tests for multiple statistical comparisons between groups were performed with Fisher's PLSD or Sidak's tests for significance, as indicated in the figure legends. In all statistical tests, significance was set at $p < .05$.

3 | RESULTS

3.1 | Cyclin D3 deficiency enhances the response of skeletal muscle to stressful stimuli

We have previously shown that cyclin D3 knockout mice display an increased number of myofibers with higher oxidative capacity in fast-twitch muscles, primarily composed of glycolytic myofibers.[19] Since adult myofibers remain plastic and can remodel their metabolic and contractile states in response to environmental demands,[41] we wished to evaluate how cyclin D3 absence would affect the response of adult muscle to adaptive stimuli such as exercise or food deprivation.

Exercise training is known to transform preexisting fast glycolytic fibers to an oxidative phenotype.[42] To explore the influence of cyclin D3 inactivation on fiber-type switching in response to exercise, 5-month-old cyclin D3 knockout mice and age-matched *WT* littermates (hereafter referred to as $D3^{-/-}$ and $D3^{+/+}$, respectively) were provided free access to a running wheel for 17 days so that they can exercise voluntarily. The wheel running activity was recorded as kilometers run during the whole 17-day period. We verified that the total distances run by $D3^{-/-}$ and $D3^{+/+}$ mice were quite comparable. At the end of the training, mice were sacrificed and tibialis anterior (TA) muscles were stained for the activity of the oxidative enzyme NADH tetrazolium reductase (NADH-TR), which is low in glycolytic fibers and progressively higher in more oxidative fibers. In parallel, we examined TA muscles from sex- and age-matched $D3^{-/-}$ and $D3^{+/+}$ mice not exposed to the running wheel as sedentary control mice (Figure 1A). Quantification of the number of fibers displaying intense, intermediate, or low staining showed a significant increase in intensely stained (dark), highly oxidative fibers, and a concomitant decrease in lightly stained (pale), glycolytic fibers within TA muscles of sedentary $D3^{-/-}$ mice compared with the relative $D3^{+/+}$ controls (Figure 1B).

For both genotypes, the comparison between rest and post-exercise conditions revealed a significantly higher

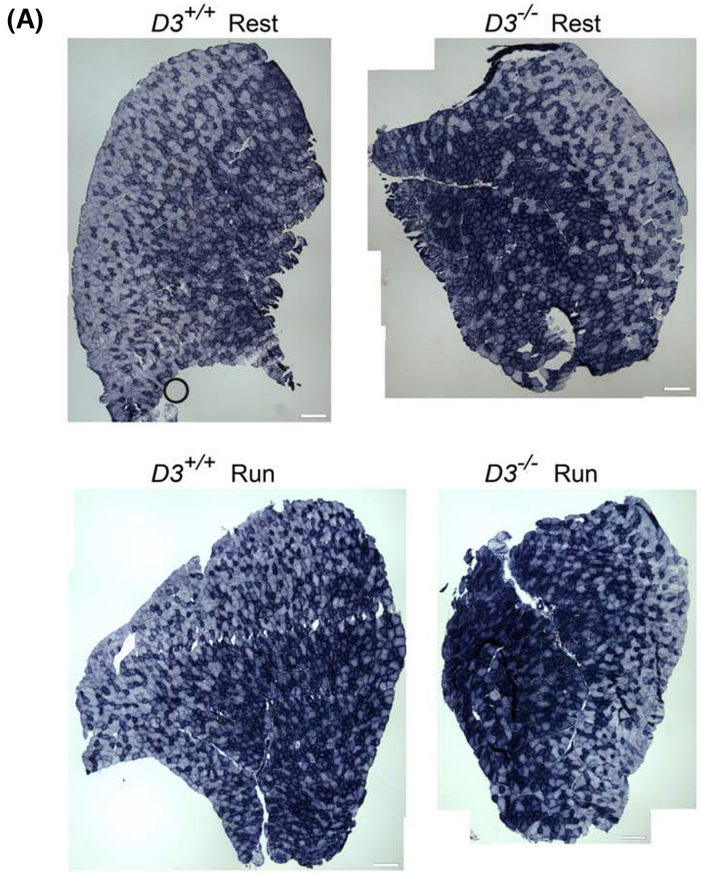

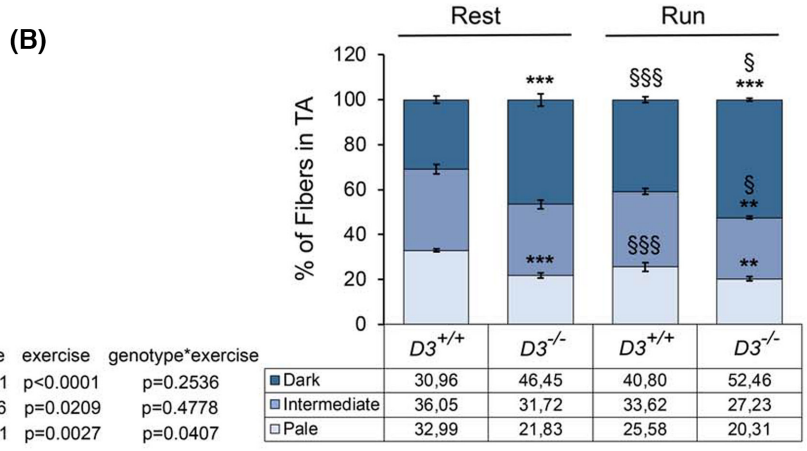

genotype	exercise	genotype*exercise
p<0.0001	p<0.0001	p=0.2536
p=0.0006	p=0.0209	p=0.4778
p<0.0001	p=0.0027	p=0.0407

	$D3^{+/+}$	$D3^{-/-}$	$D3^{+/+}$	$D3^{-/-}$
Dark	30,96	46,45	40,80	52,46
Intermediate	36,05	31,72	33,62	27,23
Pale	32,99	21,83	25,58	20,31

FIGURE 1 Loss of cyclin D3 promotes a shift in fiber type toward a more oxidative phenotype, both in basal conditions and after voluntary exercise. (A) Representative NADH-TR staining on transversal sections of TA muscle from 5-month-old, male, $D3^{+/+}$ and $D3^{-/-}$ mice exposed to a running wheel for 17 days (Run) or sedentary (Rest). (B) Quantification of the number of differentially stained NADH-TR-positive fibers in whole TA muscle sections. The data in graph are expressed as the percentage in each category of the total number of fibers per section and are presented as means ± SEM. Quantification was carried out in at least three sections per individual mouse (Run: $n = 4$ mice/genotype; Rest: $n = 3$ mice/genotype). Statistical differences were assessed by two-way ANOVA analysis (p values of each variable effect are shown next to the data table). Post hoc tests for multiple statistical comparisons between groups were performed by Fisher's PLSD test (***$p < .001$; **$p < .01$ for $D3^{-/-}$ vs. $D3^{+/+}$; §$p < .05$; §§§$p < .001$ for Run vs. Rest). Scale bar: 200 μm.

proportion of more oxidative fibers, accompanied by a lower proportion of fibers displaying low or intermediate staining (Figure 1B). Therefore, we can conclude that cyclin D3 constitutive inactivation drives the transition of muscle fibers toward a more oxidative phenotype in basal conditions, and such effect is further enhanced in the adult in response to voluntary exercise training.

To assess whether cyclin D3 loss can alter the response to food deprivation, we submitted 5-month-old $D3^{-/-}$ and $D3^{+/+}$ mice to 24 h of fasting (Figure 2). Mice were then sacrificed and quadriceps muscles were subjected to a gene expression analysis. Firstly, we measured the mRNA expression levels of cyclin D3 along with those of the family member cyclin D1. In fed conditions, we observed an increase in cyclin D1 mRNA levels in $D3^{-/-}$ compared to $D3^{+/+}$ muscle, suggesting a possible compensatory effect (Figure 2A). Both D-type cyclins transcripts were significantly downregulated upon fasting, which was expected since their protein products are known to promote anabolic pathways by mediating the response to growth factors, nutrients, and hormones.[24] Next, we examined the mRNA levels of genes that are known to respond to fasting, such as pyruvate dehydrogenase kinase isozyme 4 (PDK4), Unc-51-like kinase 1 (ULK1), encoding an upstream component

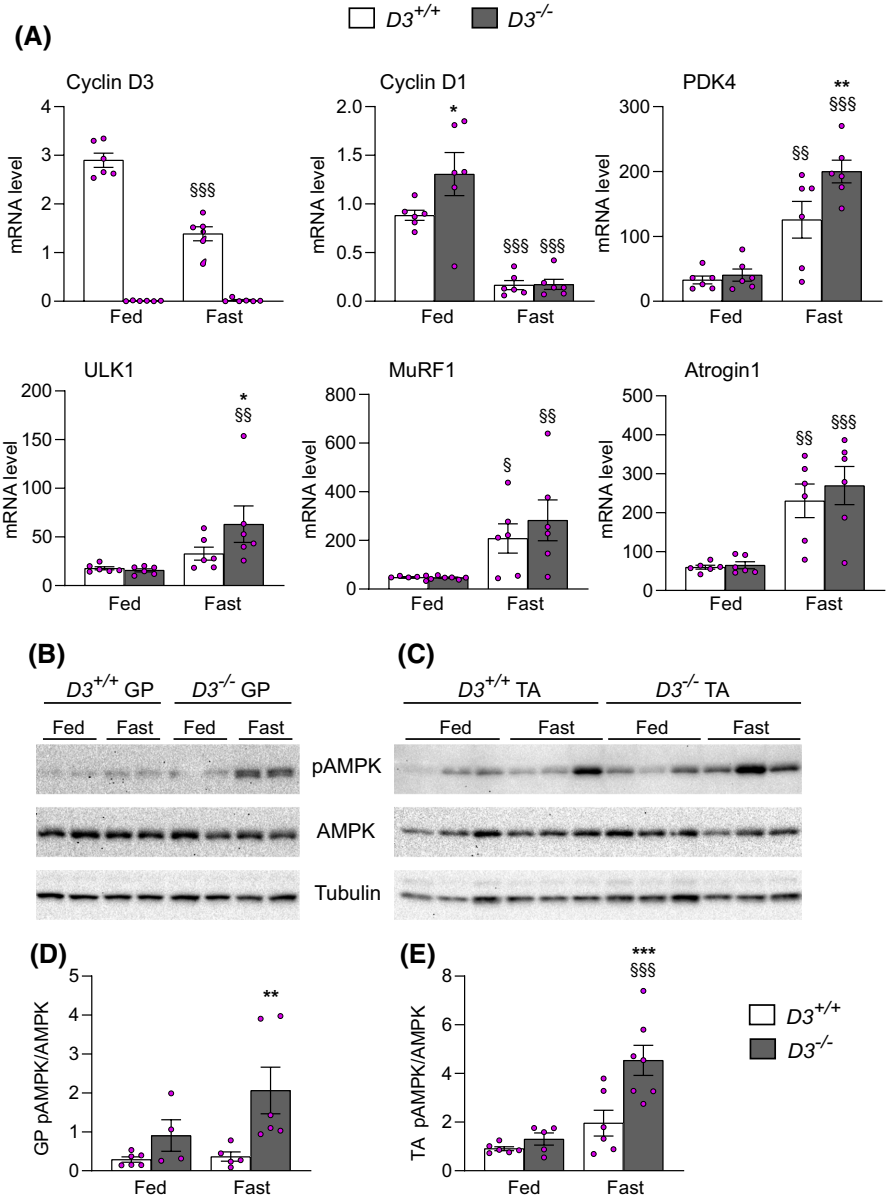

FIGURE 2 Effects of cyclin D3 ablation on the response to fasting. (A) mRNA expression of the indicated low-nutrient-responsive genes in quadriceps muscles from 5-months-old male $D3^{+/+}$ and $D3^{-/-}$ mice subjected or not to 24 h of fasting. mRNA levels were normalized to those of TBP (TATA-binding protein), used as endogenous control, and are expressed as 2^−ΔCT values. The data in graphs are presented as means ± SEM of $n = 6$ mice/group. Statistical differences were assessed by two-way ANOVA (effect of genotype: PDK4 $p = .0301$; and effect of fasting: cyclin D1 $p < .0001$, cyclin D3 $p < .0001$, PDK4 $p < .0001$, Ulk1 $p = .0056$, MuRF1 $p = .0010$, and atrogin $p < .0001$). (B, C) Representative western blots of whole protein lysates of gastrocnemius/plantaris (GP) and tibialis anterior (TA) muscles isolated from 5-month-old $D3^{+/+}$ and $D3^{-/-}$ mice in feeding or 24 h fasting conditions. Antibodies used were phospho-Thr^{172} AMPKα, total AMPKα, and Tubulin. (D, E) Densitometry analysis of band intensity from western blot analyses. The data in graphs are expressed as the ratio of phospho-Thr^{172} AMPK/t AMPKα in GP (D) and TA muscles (E) and are reported as means ± SEM of $n = 6$ mice/group. Statistical differences were assessed by two-way ANOVA (effect of genotype: GP $p = .0084$, TA $p = .0048$; effect of fasting: GP $p = .1310$, TA $p = .0002$; and interaction genotype*fasting: GP $p = .1816$, TA $p = .0313$). Post hoc tests for pairwise comparisons between groups were performed by Fisher's PLSD test. (*): $D3^{-/-}$ versus $D3^{+/+}$, $^{*}p < .05$, $^{**}p < .01$, and $^{***}p < .001$; (§): Fast versus Fed, $^{§}p < .05$, $^{§§}p < .01$, and $^{§§§}p < .001$.

of the autophagy pathway,[43] and muscle-specific RING finger protein-1 (MuRF1) and atrogin-1, encoding the two E3 ubiquitin ligases that drive the process of proteasome-mediated muscle protein degradation.[44,45] Under fasting conditions, the mRNA levels of PDK4 and ULK1 were significantly induced in $D3^{-/-}$ muscle compared with $D3^{+/+}$ muscle. Also, the levels of MuRF1 and atrogin-1 transcripts tended to be higher in $D3^{-/-}$ muscle than those observed in $D3^{+/+}$ muscle (Figure 2A). Furthermore, we examined by western blot the levels and activation state of

the AMP-activated protein kinase (AMPK), a fundamental energy sensor that is activated where nutrients are scarce to promote catabolic pathways and inhibit anabolic pathways.[46] Following 24 h of fasting, we observed a significant increase in the levels of the activated catalytic subunit of AMPKα, phosphorylated at Thr172, in protein extracts of TA and gastrocnemius/plantaris (GP) muscles from $D3^{-/-}$ compared with $D3^{+/+}$ mice. (Figure 2B–E).

Thus, cyclin D3-deficient muscle appears to adapt to fasting more efficiently than $D3^{+/+}$ muscle.

3.2 | Lack of cyclin D3 in *mdx* mice ameliorates the phenotype of muscular dystrophy

It has long been known that fast glycolytic muscle fibers are more susceptible to degeneration in Duchenne muscular dystrophy (DMD) in comparison with slower, oxidative fibers.[8,9] Based on our previous data showing that cyclin D3 inactivation stimulates the slow, oxidative myofiber program,[19] we hypothesized that ablation of cyclin D3 may promote beneficial adaptations of dystrophic muscle. To evaluate the impact of cyclin D3 deficiency in a dystrophic background, $D3^{+/-}$ mice were crossed with *mdx* mice, the mouse model of DMD, and several indicators of muscle pathology were examined in the $mdx/D3^{+/+}$ and $mdx/D3^{-/-}$ progeny.

Firstly, we analyzed the expression of adult myosin heavy-chain (MHC) isoforms and the activity of NADH-TR in TA and EDL (extensor digitorum longus) muscles from 8- to 10-week-old $mdx/D3^{-/-}$ compared with age-matched $mdx/D3^{+/+}$ animals (Figure 3). Coimmunostaining with anti-MHC-2a and anti-MHC-2x antibodies enabled identification of fibers expressing type 2a (green), type 2x (red), or both type 2a/2x MHC, whereas the unstained fibers essentially represented fibers expressing exclusively type 2b MHC, the fastest isoform of MHC, as the number of slow MHC-I fibers is extremely low in TA and EDL muscles (Figure 3A,C). Quantification data revealed a significant decrease in the percentage of unstained fibers expressing MHC-2b in both TA and EDL muscles from $mdx/D3^{-/-}$ *mice*. This was accompanied by a reciprocal increase in the percentage of fibers expressing slower isoforms of MHC, namely MHC-2a in TA and MHC-2x in EDL muscles, respectively (Figure 3B,D). The above data clearly indicate a progressive fiber-type transition in the direction 2b → 2x → 2a in both the EDL and TA fast-twitch muscles of $mdx/D3^{-/-}$ mice compared with $mdx/D3^{+/+}$ mice. Furthermore, histochemical staining for NADH-TR activity showed increased staining intensities of NADH-TR-positive fibers in both TA and EDL of *mdx* mice lacking cyclin D3 compared with $mdx/D3^{+/+}$ muscles (Figure 3E–H), which reflects more oxidative fibers and enhanced mitochondrial activity. Therefore, lack of cyclin D3 in the *mdx* genetic background promotes a fast-to-slow and glycolytic-to-oxidative fiber-type shift, similar to what was observed previously in non-dystrophic mice.[19]

Since it is known that one of the major compensatory metabolic changes that occurs in dystrophic muscle is a transition to slow fiber type,[2] we compared the effects of cyclin D3 ablation on the expression of adult MHC isoforms in TA muscles of *mdx* versus non-dystrophic mice (Supporting Information Figure S1A). As expected, ablation of cyclin D3 or the *mdx* mutation independently caused a fast-to-slow shift (see comparisons $D3^{-/-}$ vs. $D3^{+/+}$ and $mdx/D3^{+/+}$ vs. $D3^{+/+}$). However, ablation of cyclin D3 in the *mdx* genetic background promoted a further progression toward a slower fiber type compared with that induced in non-dystrophic background. In fact, $mdx/D3^{-/-}$ muscles displayed a reduced number of fibers expressing the fastest isoform of MHC (MHC-2b) and an increased number of fibers expressing slower MHC isoforms (i.e., MHC-2x fibers and hybrid fibers coexpressing MHC-2a and MHC-2x). Similarly, staining for NADH-TR activity showed a progressive transition from glycolytic (pale) toward more oxidative myofibers (intermediate) in dystrophic muscle from $mdx/D3^{-/-}$ mice compared to $D3^{-/-}$ non-dystrophic muscle (Supporting Information Figure S1B). Therefore, the absence of cyclin D3 appears to enhance the beneficial adaptation toward a slower more oxidative fiber type naturally occurring in *mdx* muscles.

Next, we analyzed several hallmarks of muscle pathology in TA muscles from $mdx/D3^{-/-}$ mice compared with age-matched $mdx/D3^{+/+}$ mice at different stages of disease progression (5 weeks, 2 months, and 5 months of age). At 5 weeks of age, staining with hematoxylin–eosin and anti-mouse IgG/IgM revealed evident muscle damage with several necrotic areas containing IgG/IgM-positive fibers surrounded by infiltrating mononuclear cells, whereas staining against the F4/80 macrophage marker showed infiltration of immune cells (Figure 4A). Quantitative analyses indicated a reduced extent of IgG/IgM-positive and F4/80-positive areas in dystrophic muscles lacking cyclin D3 compared with muscles from *mdx* littermate controls (Figure 4B,C). At 2 and 5 months of age, the degree of myofiber necrosis was evaluated by determining the intracellular presence of IgG and IgM on muscle sections, as an indicator of the structural integrity of sarcolemma (Figure 4D). The percentage of IgG/IgM-positive fibers over the total number of fibers in muscles from $mdx/D3^{-/-}$ mice was lower than that seen in $mdx/D3^{+/+}$ mice (Figure 4E). Furthermore, at 2 months of age, we also evaluated inflammatory infiltration and extracellular matrix deposition by F4/80 and Sirius red staining, respectively (Supporting Information Figure S2). While the extent of macrophage infiltration was lower than

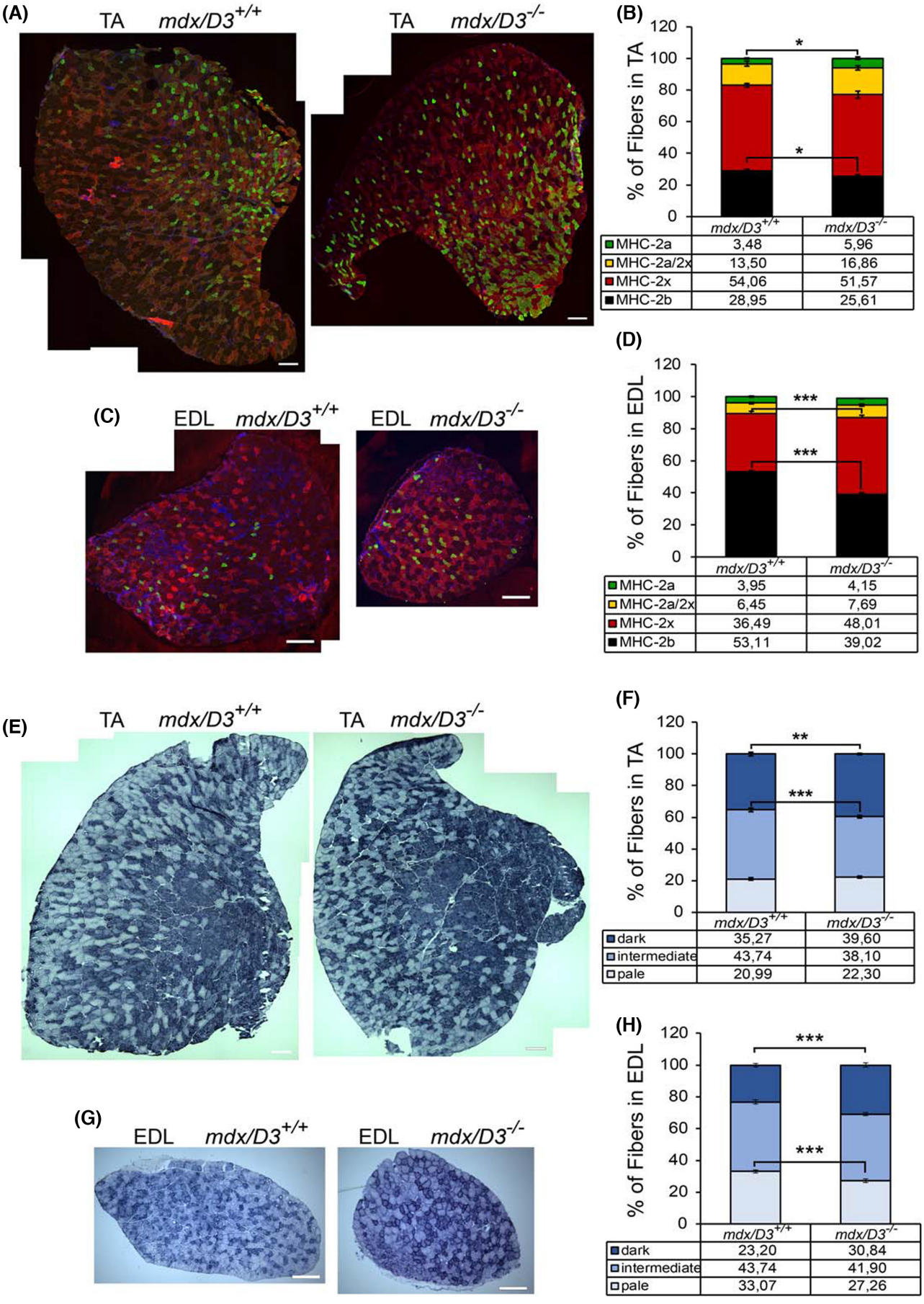

FIGURE 3 *mdxD3*$^{-/-}$ mice display shifts in fiber type toward a slower, more oxidative phenotype. (A, C) Representative transverse sections of TA and EDL muscles of 8- to 10-week-old *mdx/D3*$^{-/-}$ and *mdx/D3*$^{+/+}$ mice coimmunostained for MHC-2a (green) and MHC-2x (red) and counterstained with Hoechst. (B, D) Number of fibers expressing MHC-2a, MHC-2x, MHC-2a/2x, or MHC-2b (unstained fibers) in TA and EDL sections, respectively. Data are expressed as the percentage in each category of the total number of fibers per section and are presented as means ± SEM (TA: $n = 5$ *mdx/D3*$^{+/+}$, $n = 6$ *mdx/D3*$^{-/-}$; EDL: $n = 6$ mice/genotype). (E, G) Histochemical staining of NADH-TR enzymatic activity in TA and EDL transverse sections of 8- to 10-week-old *mdx/D3*$^{-/-}$ and *mdx/D3*$^{+/+}$ mice. (F, H) Number of differentially stained (dark, intermediate, or pale) NADH-TR-positive fibers in TA and EDL muscle sections. Data are expressed as the percentage in each category of the total number of fibers per section and are presented as means ± SEM ($n = 6$ mice/genotype). All quantification data are from at least three serial sections per individual mouse. Statistical differences between *mdx/D3*$^{+/+}$ and *mdx/D3*$^{-/-}$ mice were assessed by two-tailed unpaired Student's *t*-tests (*$p < .05$, **$p < .01$, and ***$p < .001$). Scale bar: 200 μm.

that observed at 5 weeks of age, it appeared again reduced in muscle of *mdx/D3*$^{-/-}$ mice compared with *mdx/D3*$^{+/+}$ controls (Supporting Information Figure S2A,B). In contrast, the fibrotic index did not change significantly between the *mdx/D3*$^{+/+}$ and *mdx/D3*$^{-/-}$ genotypes (Supporting Information Figure S2C,D).

Finally, we measured the frequency of newly generated myofibers expressing the embryonic isoform of myosin heavy chain (eMyHC) and the frequency of centrally nucleated myofibers, as indicators of the amount of damage-induced regeneration. At each age analyzed, we observed a reduced degree of eMyHC expression and central nucleation in muscles from *mdx/D3*$^{-/-}$ compared with *mdx/D3*$^{+/+}$ mice, which indicates reduced degenerative/regenerative processes during disease progression in *mdx* muscles lacking cyclin D3 (Figure 4F–H).

Among several morphological abnormalities, dystrophic muscle fibers are known to display a greater variation in their cross-sectional area due to the presence of increased numbers of small regenerating myofibers and very large hypertrophic myofibers.[39] This histological hallmark of muscular dystrophy, together with the percentage of centralized nuclei, reflects the ongoing degeneration/regeneration of dystrophic muscle fibers. Therefore, we measured the cross-sectional area (CSA) of single myofibers in TA muscles from 2-month-old *mdx/D3*$^{+/+}$ and *mdx/D3*$^{-/-}$, and in parallel, we also analyzed TA muscles from age-matched non-dystrophic mice (*WT*: C57BL10). Then, we constructed a size distribution histogram (Figure 5A) and quantified the heterogeneity of muscle fiber size by calculating a variance coefficient of fiber size (Figure 5B,C). As expected, the CSA variance coefficient increased in the *mdx* genetic background. However, muscles from *mdx/D3*$^{-/-}$ mice displayed a significant reduction in fiber area variability compared with *mdx/D3*$^{+/+}$ mice (Figure 5B). A similar result was obtained using the minimal Feret's diameter as the geometrical parameter of fiber size (Figure 5C).

Overall, the above data indicate that inactivation of cyclin D3 can ameliorate multiple aspects of dystrophic muscle histopathology.

3.3 | Functional analysis of dystrophic muscle lacking cyclin D3

We then evaluated whether cyclin D3 inactivation may improve dystrophic muscle function. To this end, TA muscles of 4-month-old *mdx/D3*$^{-/-}$ mice or *mdx/D3*$^{+/+}$ mice were analyzed in situ for a number of contractile parameters (Table 1, Figure 6).

TA muscles from *mdx/D3*$^{-/-}$ mice generated an absolute tetanic force significantly lower than *mdx/D3*$^{+/+}$ muscles. However, following normalization for muscle cross-sectional area, the specific tetanic force of TA muscles did not change significantly between the two genotypes. Likewise, no significant differences were observed in the twitch force, the time-to-peak tension, and the half relaxation time (Table 1). Conversely, the maximal rate of twitch force relaxation (-dF/dt) was significantly slower in *mdx/D3*$^{-/-}$ mice compared with *mdx/D3*$^{+/+}$ control littermates, and the maximal rate of twitch force development (+dF/dt) also tended to be slower (Table 1, Figure 6A). This result suggests that the absence of cyclin D3 induced a slowing down in the contractile kinetics, which in turn might be related to a shift of the overall fiber-type composition toward a slower phenotype.

Furthermore, we determined the degree of TA muscle susceptibility to damage by measuring the drop in force produced during repetitive electrically stimulated eccentric contractions. Notably, *mdx/D3*$^{-/-}$ muscles displayed a consistently reduced force drop during repeated stimulations compared to control muscles. After eight stimulations, the maximal force generated by *mdx/D3*$^{++}$ muscles was reduced to about 35% of the initial force, on average, whereas the force produced by cyclin D3-deficient *mdx* muscles maintained about 66% of their initial force (Figure 6B). This result suggests that the absence of cyclin D3 might contribute to protecting muscle from mechanical damage and fatigability, a result in accordance with a shift toward a slower and more resistant to fatigue phenotype.

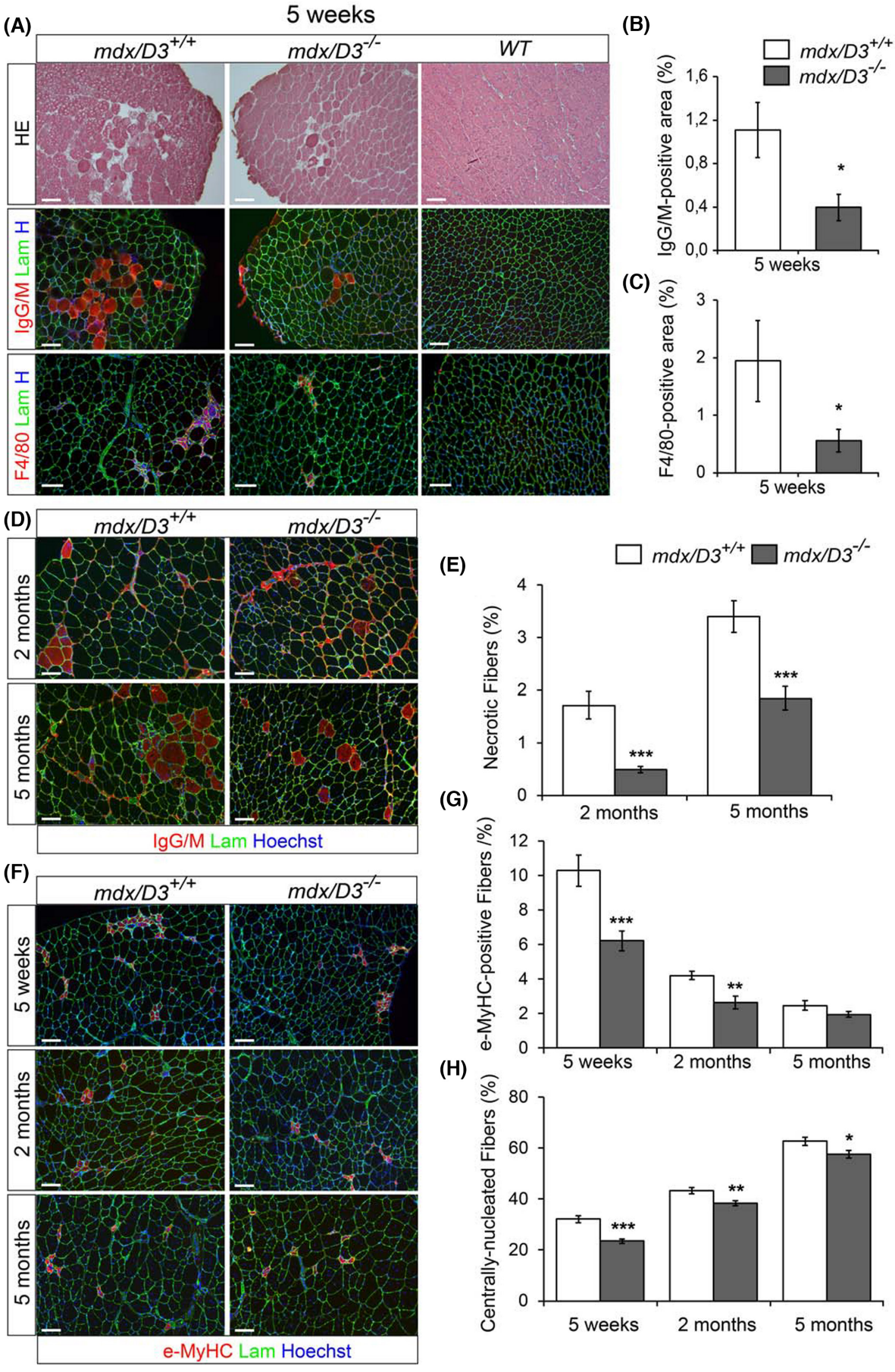

FIGURE 4 Loss of cyclin D3 improves dystrophic muscle histopathology. (A) Transversal sections of TA muscles from 5-week-old *mdx/D3*$^{-/-}$ *mdx/D3*$^{+/+}$ and *WT* mice stained with hematoxylin–eosin or coimmunostained with anti-IgG/IgM antibody (red) and anti-laminin (green), or coimmunostained with anti-F4/80 (red) and anti-laminin (green), as indicated. (B, C) Extent of IgG/IgM-positive and F4/80-positive areas expressed as the percentage of the total TA cross-sectional area. Data are presented as means ± SEM (*mdx/D3*$^{+/+}$: $n = 4$, *mdx/D3*$^{-/-}$: $n = 5$). (D) TA sections from 2- and 5-month-old *mdx/D3*$^{-/-}$ and *mdx/D3*$^{+/+}$ mice coimmunostained with anti-IgG/IgM antibody (red) and anti-laminin (green), and counterstained with Hoechst. (E) Number of IgG/IgM-positive fibers expressed as the percentage of the total number of myofibers per section. Data are presented as means ± SEM (2 months: $n = 6$ *mdx/D3*$^{+/+}$, $n = 5$ *mdx/D3*$^{-/-}$; 5 months: $n = 6$ mice/genotype). (F) TA sections from 5-week-, 2-month-, and 5-month-old *mdx/D3*$^{-/-}$ and *mdx/D3*$^{+/+}$ mice coimmunostained for embryonic myosin heavy chain (eMyHC, red) and laminin (green). Nuclei were visualized by counterstaining with Hoechst. (G, H) Number of eMyHC-positive and number of centrally nucleated myofibers, respectively, expressed as the percentage of the total number of fibers counted in entire TA cross sections. Data are presented as means ± SEM (5 weeks: n = 5 mice/genotype; 2 months: $n = 5$ mice/genotype; 5 months: $n = 6$ mdx/D3$^{+/+}$, $n = 7$ mdx/D3$^{-/-}$). All quantification data are from at least three serial sections per individual mouse. Asterisks above histograms denote statistical significance by Mann–Whitney U test (panels B, E) or by two-tailed unpaired Student's *t*-test (panels C, G, H): $^{*}p < .05$; $^{**}p < .01$; and $^{***}p < .001$. Scale bar: 100 μm.

3.4 | Lack of cyclin D3 in *mdx* mice preserves endurance exercise performance

Next, we asked whether the improvement in muscle histopathology and function observed in *mdx/D3*$^{-/-}$ mice resulted in better performance in a fatigue resistance exercise paradigm. Repeated treadmill exercises are routinely used to increase myofiber necrosis and accelerate muscle weakness in *mdx* mice to more closely mirror the muscle pathology seen in patients with DMD. Therefore, 4-month-old *mdx/D3*$^{-/-}$ and *mdx/D3*$^{+/+}$ control mice were subjected to forced exercise on an accelerating treadmill. On each trial, the exercise continued until exhaustion and was repeated once a week for 5 consecutive weeks. A group of *WT* mice was also included as a reference healthy control (Figure 7). The performance of dystrophic mice was significantly lower than that seen in *WT* mice; however, *mdx/D3*$^{-/-}$ mice performed significantly better than *mdx/D3*$^{+/+}$ mice, as they displayed over the five exercise sessions a cumulative running time of 130 min compared to the 82 min mean performance of *mdx/D3*$^{+/+}$ (Figure 7A). Furthermore, we analyzed the data recorded in each exercise trial, also taking into account body weight as a covariate. Although the initial performance was very similar between the two genotypes, the time to exhaustion was progressively reduced in *mdx/D3*$^{+/+}$ mice during each of the succeeding trials while remaining unaltered in *mdx/D3*$^{-/-}$ mice (Figure 7B).

Therefore, cyclin D3 deficiency appears to result in enhanced tolerance to exhaustion training.

3.5 | Lack of cyclin D3 in *mdx* mice boosts muscle regeneration and oxidative metabolism following exercise

To evaluate the effects of endurance exercises on muscle damage and regeneration, *mdx/D3*$^{-/-}$ and *mdx/D3*$^{+/+}$ control mice were sacrificed after the last bout of exercise, and GP muscles were dissected and stained for anti-mouse IgG/IgM and anti-eMyHC antibodies. Parallel analyses were carried out on sections from GP muscles isolated from age-matched mice that were not exposed to the treadmill running protocol (Rest) (Figure 8A).

Quantification data indicated a significant reduction in IgG/IgM-positive "degenerating area" in exercised *mdx/D3*$^{-/-}$ mice compared with the corresponding *mdx/D3*$^{+/+}$ control mice, whereas the difference between the two genotypes was slightly below significance in resting conditions. No signs of myofiber necrosis were detectable in GP muscles from sedentary or exercised *WT* mice (data not shown). As for regeneration, the eMyHC-positive area was significantly lower in *mdx/D3*$^{-/-}$ mice than that measured in *mdx/D3*$^{+/+}$ mice in sedentary conditions. In contrast, running induced a significant increase in regenerating area in *mdx/D3*$^{-/-}$ mice, of about 30% compared with exercised (Run) *mdx/D3*$^{+/+}$ controls, and threefold compared with Rest *mdx/D3*$^{-/-}$ mice. The extent of regeneration was not significantly different between Rest and Run *mdx/D3*$^{+/+}$ animals (Figure 8B).

Therefore, the absence of cyclin D3 appears to result in reduced susceptibility of dystrophic muscle to injury and enhanced regenerative capacity in response to exercise.

To explore whether the exercise regimen to which the mice were subjected affected the metabolic profile of muscle fibers, GP muscles from *mdx/D3*$^{+/+}$ and *mdx/D3*$^{-/-}$ exercised and age-matched sedentary mice were stained for the activity of the oxidative enzyme NADH-TR (Figure 8C). Results showed a significant increase in intensely stained (dark), highly oxidative fibers in muscles of both Rest and Run *mdx/D3*$^{-/-}$ mice compared with the relative *mdx/D3*$^{+/+}$ controls. Exercised *mdx/D3*$^{-/-}$ mice also displayed a significant decrease in lightly stained (pale), glycolytic fibers. The comparison between rest and post-exercise conditions revealed a significantly lower proportion of glycolytic (pale) fibers in both genotypes,

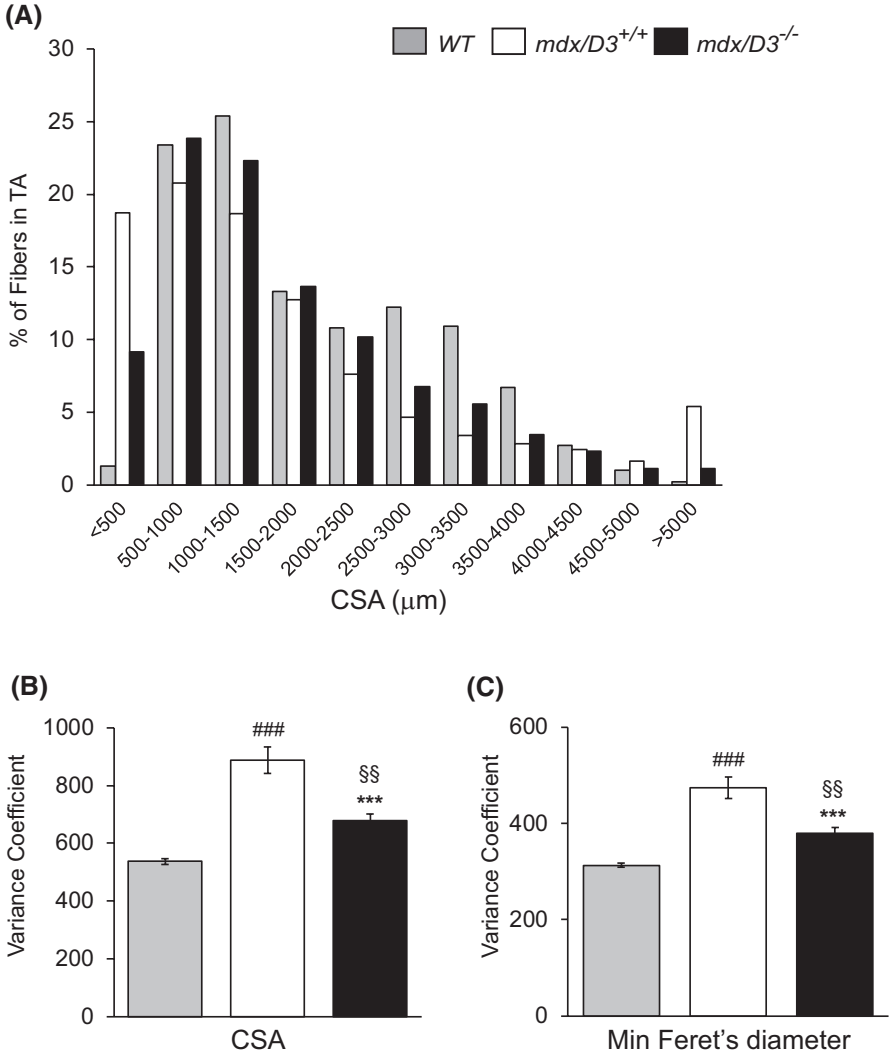

FIGURE 5 Lack of cyclin D3 in *mdx* mice reduces muscle fiber size variability. (A) Frequency histogram showing the myofiber cross-sectional area (CSA) measured on transverse sections of TA muscle from 2-month-old male *mdx/D3*$^{-/-}$, *mdx/D3*$^{+/+}$, and *WT* non-dystrophic (C57BL10) mice (WT: $n = 4421$ myofibers, *mdx/D3*$^{+/+}$: $n = 6127$ myofibers, and *mdx/D3−/−*: $n = 6124$ myofibers measured in three TA serial sections from three mice per experimental group). Note that small-caliber and large-caliber fibers are more abundant in dystrophic muscles. (B, C) Variance coefficient of the fiber size in TA cross-sections calculated using two geometrical parameters: CSA (B) and minimal Feret's diameter (C). The variance coefficients were calculated by multiplying the standard deviation of all measurements by 1000 and dividing it by the mean fiber size. Data are presented as means ± SEM. Statistical differences were assessed by one-way ANOVA ($p < .0001$) followed by Fisher's PLSD post hoc tests for comparisons between genotypes. (*****): *mdx/D3*$^{-/-}$ versus *mdx/D3*$^{+/+}$, ***$p < .001$; (#): *mdx/D3*$^{+/+}$ versus *WT*, $^{\#\#\#}p < .001$; (§): *mdx/D3*$^{-/-}$ versus *WT*, $^{\S\S}p < .01$.

and this was accompanied in *mdx/D3*$^{-/-}$ by a significantly higher proportion of fibers displaying intermediate staining. Therefore, running induced shifts in fiber type toward a more oxidative phenotype that appeared more accentuated in dystrophic muscles lacking cyclin D3.

Furthermore, we performed a gene expression analysis on quadriceps muscles from *mdx/D3*$^{+/+}$, *mdx/D3*$^{-/-}$, and *WT* healthy control mice in resting and post-exercise conditions (Figure 9). The results confirmed an enhancement of regeneration in muscles from cyclinD3-deficient *mdx* mice compared to *mdx* control mice in post-exercise conditions. In fact, the mRNA levels of *MYH3*, the gene encoding e-MyHC, were significantly boosted in *mdx/D3*$^{-/-}$ over those detected in *mdx/D3*$^{+/+}$ mice in post-exercise conditions, and those of the myogenic regulatory gene, myogenin, significantly increased in exercised versus rest *mdx/D3*$^{-/-}$ mice, but not in the corresponding *mdx/D3*$^{+/+}$ mice.

We also examined the mRNA expression levels of a number of genes encoding factors involved in the regulation of oxidative metabolism and oxidative stress in response to exercise, such as the transcriptional coactivator PGC1α[47], the transcription factors PPARδ[48] and nuclear factor erythroid 2-related factor 2 (NEF2L2, better known

TABLE 1 Contractile properties of tibialis anterior muscles of *mdx/D3*$^{+/+}$ and *mdx/D3*$^{-/-}$ mice.

	mdx/D3$^{+/+}$	*mdx/D3*$^{-/-}$
Muscle mass (mg)	65.36 ± 5.20	44.63 ± 3.68 ***
Muscle CSA (mm^2)[a]	8.55 ± 0.66	6.70 ± 0.56 (p = .054)
Twitch		
Twitch force (mN)	157.56 ± 10.95	123.37 ± 13.02 (p = .067)
Specific twitch force (mN/mm^2)	18.92 ± 1.51	18.67 ± 1.72
TTP (ms)[b]	32.74 ± 2.20	37.89 ± 3.61
½ RT (ms)[c]	28.93 ± 6.07	30.71 ± 4.85
dF/dt (mN/ms)[d]	10.64 ± 1.05	7.80 ± 1.05 (p = .079)
−dF/dt (mN/ms)[e]	5.88 ± 0.78	3.55 ± 0.49*
Tetanus		
Tetanic force (mN)	525.85 ± 38.13	370.54 ± 39.01*
Specific tetanic force (mN/mm^2)	64.33 ± 7.55	56.24 ± 5.45

Note: Force measurements were performed in situ on tibialis anterior muscles of 4-month-old *mdx/D3*$^{-/-}$ and *mdx/D3*$^{+/+}$ mice. Values shown are means ± SEM (n = 7 mice/genotype). Significant differences between *mdx/D3*$^{+/+}$ and *mdx/D3*$^{-/-}$ mice were assessed by two-tailed unpaired t-tests. Tetanic force: absolute maximum isometric force measured in milliNewtons; Twitch force: maximum force of twitch, measured in milliNewtons; Specific tetanic force and specific twitch force were obtained after normalization to muscle CSA, milliNewtons per square millimeters.

[a]CSA: cross-sectional area expressed in square millimeters.

[b]TTP: time to peak twitch force, measured in milliseconds.

[c]½ RT: half relaxation time of twitch, milliseconds.

[d]dF/dt: maximal rate of twitch force development, milliNewtons per milliseconds.

[e]−dF/dt: maximal rate of twitch force relaxation, milliNewtons per milliseconds.

*p < .05; ***p < .001.

as NRF2),[49] uncoupling protein 2 (UCP2),[50] and superoxide dismutase 3 (SOD3).[51] In addition, we measured the utrophin gene transcripts (Utrn) whose levels are known to be higher in oxidative muscle fibers[55] (Figure 9). The expression of PPARδ mRNA significantly increased in post-exercise conditions, but no differences were observed between *mdx/D3*$^{+/+}$ and *mdx/D3*$^{-/-}$ muscles. Remarkably, however, the gene transcripts of PGC1α, a master regulator of mitochondrial biogenesis,[52] were significantly induced in muscles from exercised *mdx/D3*$^{-/-}$ mice compared to the relative *mdx/D3*$^{+/+}$ or *WT* healthy controls, which revealed an effect of cyclin D3 ablation on PGC1α gene expression during states that require increased energy, such as exercise. Likewise, the transcripts encoding UCP2, a mitochondrial protein that decreases production of reactive oxygen species by mild uncoupling of oxidative phosphorylation,[53] and NRF2, a master regulator of the antioxidant response,[54] were significantly increased in exercised *mdx/D3*$^{-/-}$ compared with the corresponding *mdx/D3*$^{+/+}$ muscles. The mRNA expression of SOD3, a target gene of NRF2,[54] significantly increased in exercised versus rest *mdx/D3*$^{-/-}$ mice, but not in the corresponding *mdx/D3*$^{+/+}$ mice. Finally, the mRNA levels of Utrn significantly increased in dystrophic muscles in response to exercise and appeared significantly higher in exercised *mdx/D3*$^{-/-}$ mice relative to the corresponding *mdx/D3*$^{+/+}$ mice.

In contrast to the gene transcripts measured in quadriceps muscles, no significant changes were observed in the steady-state protein levels of PGC1α and NRF2 in GP muscles of exercised versus resting *mdx/D3*$^{+/+}$ and *mdx/D3*$^{-/-}$ mice (Figure 10A,B). We also measured the utrophin protein levels in TA muscles from sedentary or exercised mice (Figure 10C,D). In both conditions, *mdx/D3*$^{+/+}$ and *mdx/D3*$^{-/-}$ muscles were found to express significantly higher levels of utrophin compared with *WT* muscles, which was expected since utrophin is known to be naturally upregulated in dystrophic muscle.[2] However, no significant differences in utrophin protein content were found between the two genotypes in either condition (Figure 10).

4 | DISCUSSION

We previously showed that cyclin D3 knockout mice display a slower, more oxidative muscle phenotype, with effects on whole organism energy metabolism. Furthermore, we provided evidence suggesting that cyclin D3 may control the slow, oxidative fiber-specific gene program by modulating the activity of MEF2 and/or NFAT transcription factors.[19]

Here, we further characterized the muscle phenotype of cyclin D3 knockout mice by examining the adaptive response to external stimuli that are known to enhance

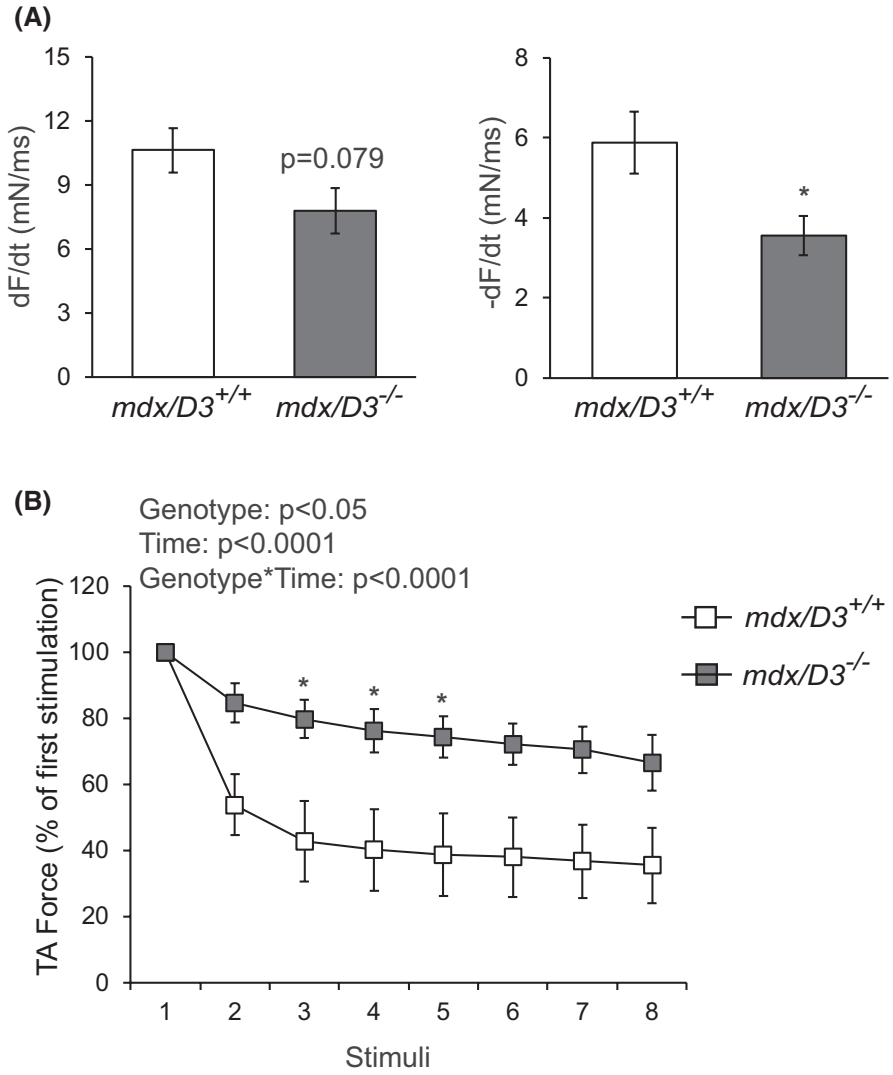

FIGURE 6 Lack of cyclin D3 in *mdx* mice improves dystrophic muscle function. (A) Maximal rate of force development (df/dT) and maximal rate of relaxation (−df/dT) measured in TA muscles of *mdx/D3*$^{+/+}$ and *mdx/D3*$^{-/-}$ mice following a 300 mA stimulus. Data are reported as means ± SEM. Statistical differences between *mdx/D3*$^{-/-}$ and *mdx/D3*$^{+/+}$ mice were assessed by two-tailed unpaired *t*-tests (*$p < .05$). (B) TA muscle susceptibility to damage was assessed by measuring the maximal force developed during repetitive eccentric stimulations. The value determined at each stimulation is expressed as the percentage of the value measured for each group at the first stimulation, assumed as 100%. Data are presented as means ± SEM ($n = 7$ mice for each group). Statistical significance was determined by two-way ANOVA for repeated measures (*p* value of each variable effect shown above chart). (*) indicates statistical analysis by Sidak's post hoc test in the comparison of *mdx/D3*$^{-/-}$ versus *mdx/D3*$^{+/+}$, *$p < .05$.

muscle oxidative metabolisms, such as voluntary exercise and food deprivation.[41] We show that, in addition to driving glycolytic-to-oxidative fiber-type switch in basal conditions, lack of cyclin D3 can further increase the percentage of myofibers utilizing oxidative metabolism in the adulthood following voluntary exercise.

The AMP-activated protein kinase (AMPK) is a key sensor of low cellular energy status that acts to restore energy homeostasis by promoting catabolic pathways that fuel energy production.[56] Interestingly, in response to food starvation, we observed an increase in the levels of the activated isoform of AMPKα, phosphorylated at Thr172, in muscles from *D3*$^{-/-}$ mice compared with those from *D3*$^{+/+}$ controls. Accordingly, muscles from fasted cyclin D3-deficient mice displayed a significant mRNA increase in PDK4, which limits glycolysis-derived pyruvate utilization, thus favoring the use of fatty acids as substrate for mitochondrial oxidation and ULK1, a serine–threonine kinase that initiates the autophagy process.[41]

It was recently reported that the cyclin D-dependent CDK4 kinase directly phosphorylates and inhibits the catalytic AMPKα2 subunit and that this phosphorylation is functionally relevant.[57] Importantly, in vitro kinase assays showed that recombinant CDK4/CyclinD3, but not recombinant CDK4/CyclinD1, complexes efficiently phosphorylated AMPK subunits, suggesting that AMPK phosphorylation by CDK4 requires recognition by cyclin D3. Site-directed mutagenesis identified four CDK4 phosphosites in AMPKα2. The relationships between inhibitory phosphorylations by CDK4/cyclinD3 and activating phosphorylation of Thr172 by AMPK upstream kinases remain to be elucidated; however, the results reported by Lopez-Mejia et al.[57] suggest that the CDK4-dependent phosphorylations are present in the absence of the activating Thr172 phosphorylation. Remarkably, *Cdk4*$^{-/-}$ mice displayed enhanced oxidative metabolism and exercise capacity,[57] and these alterations resemble those previously observed by us in *D3*$^{-/-}$ mice.[19] Taken together, our results and the observations above suggest that cyclin D3 deficiency may stimulate activation of the key energy and nutrient sensor AMPK by eliminating AMPK inhibition by CDK4. Future studies will further analyze targets and markers of AMPK activity in cyclinD3-null muscle.

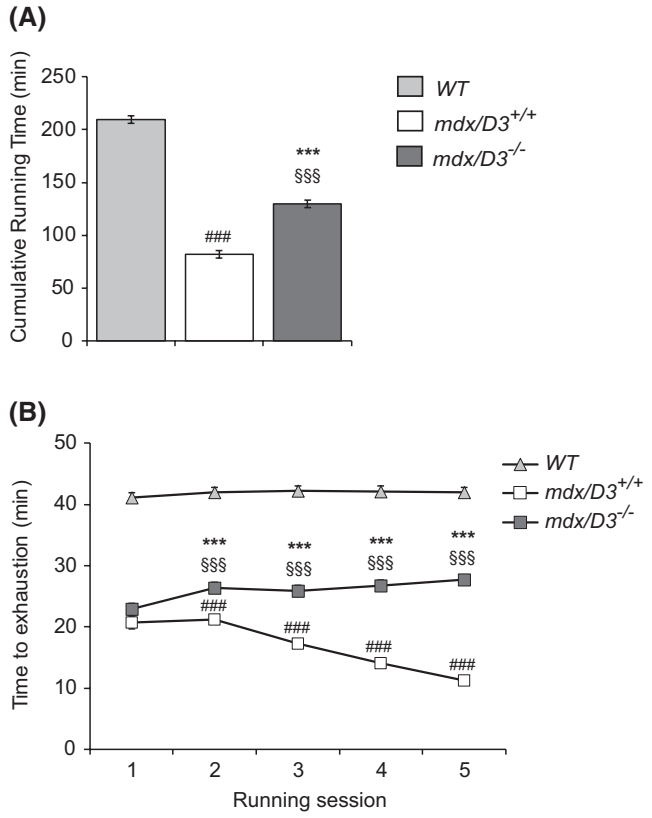

FIGURE 7 Lack of cyclin D3 in *mdx* mice improves exercise endurance. Running time was acquired in *mdx/D3*$^{-/-}$, *mdx/D3*$^{+/+}$, and *WT* (C57BL10) during five weekly treadmill trials with endurance exercise protocol. Mice were subjected to the first trial at 4 months of age. (A) Cumulative run time during the five trials. Data are reported as means ± SEM (*WT*: $n = 5$, *mdx/D3*$^{+/+}$: $n = 15$, *mdx/D3*$^{+/+}$: $n = 17$). Statistical differences were assessed by one-way ANOVA ($p < .001$). (B) Graph showing the duration of running during each trial (means ±SEM). Statistical differences were assessed by two-way ANCOVA analysis for repeated measures, using body weight as a covariate (effect of genotype: $p = .0006$; effect of time: $p = .8986$). Post hoc tests for comparisons between genotypes were performed by Fisher's PLSD test. (*****): *mdx/D3*$^{-/-}$ versus *mdx/D3*$^{+/+}$, $^{***}p < .001$; (**#**): *mdx/D3*$^{+/+}$ versus *WT*, $^{\#\#\#}p < .001$; (§): *mdx/D3*$^{-/-}$ versus *WT*, $^{§§§}p < .001$.

Concomitantly with the above studies, we evaluated the effects of cyclin D3 deficiency in the *mdx* mouse model of DMD. Several lines of evidence led us to hypothesize that inactivation of cyclin D3 could counteract DMD. Specifically, (1) it is known that slow, oxidative muscle fibers are more resistant to dystrophic degeneration compared to fast, glycolytic fibers[8,9]; (2) previous work in our lab showed that muscles from cyclin D3 knockout mice display an increased number of slower, more oxidative myofibers, and increased levels of a number of metabolic regulators including PGC1α,[19] which is known to protect from DMD.[15] In addition, data reported in the present study suggest that cyclin D3 ablation may stimulate activation of AMPK in response to energy stress, and pharmacologic activation of AMPK has been shown to beneficially alter the phenotype of dystrophic muscle.[14]

We analyzed various aspects of disease progression in *mdx/D3*$^{-/-}$ mice compared with *mdx/D3*$^{+/+}$ control littermates. Three main indicators of the dystrophic pathology, that is, fiber damage, regeneration, and size variability, were attenuated in dystrophic muscles lacking cyclin D3. Indeed, *mdx/D3*$^{-/-}$ muscles showed a reduced degree of myofiber damage compared with *mdx/D3*$^{+/+}$ control muscles, and this was accompanied by a reduced number of fibers exhibiting centrally located nuclei or expressing the embryonic isoform of myosin heavy chain. Importantly, muscles from *mdx/D3*$^{-/-}$ mice also displayed a significant reduction in fiber size variability compared with those from *mdx/D3*$^{+/+}$ mice. These results indicate reduced degenerative/regenerative processes in *mdx* muscles lacking cyclin D3. Furthermore, as previously observed in the cyclin D3 knockout mouse model, immunohistological analyses confirmed a fastest-to-slower and glycolytic-to-oxidative fiber-type transition in muscles of *mdx* mice lacking cyclin D3, which is in line with the hypothesis that cyclin D3 deficiency may drive beneficial adaptations of *mdx* muscle by promoting a slower, more oxidative myofiber profile.

Interestingly, ablation of the Nfix transcription factor in dystrophic mice has been shown to induce a muscle phenotype similar to that observed by us in *mdx/D3*$^{-/-}$ mice. In fact, in addition to promoting a shift toward a more oxidative fiber type, depletion of Nfix resulted in a delay of the regenerative process, which lead to the first proposed concept that slowing the regenerative burst may confer benefits to dystrophic muscle as a consequence of the delay of the degeneration–regeneration circuit.[18]

Muscle regeneration is a high-energy demanding anabolic process that represents a challenge for dystrophic muscle; furthermore, many of the newly generated myofibers will undergo necrosis due to the absence of dystrophin, thus feeding recurrent futile cycles of degeneration/regeneration. A widely accepted notion is that satellite cells become functionally exhausted in the chronically degenerative environment of dystrophic muscle, although it has also been shown that dystrophin-deficient muscle satellite cells are intrinsically impaired and may directly contribute to DMD pathogenesis and disease progression in *mdx* mice.[58,59]

While the reduced regeneration observed in cyclin D3-null dystrophic muscle may be attributed to the reduced extent of myofiber injury, cyclin D3 deficiency might also intrinsically affect the behavior of satellite cells. Indeed, in a previous study conducted in non-dystrophic mice, we showed that cyclin D3 plays a unique function in controlling the proliferation/differentiation balance of

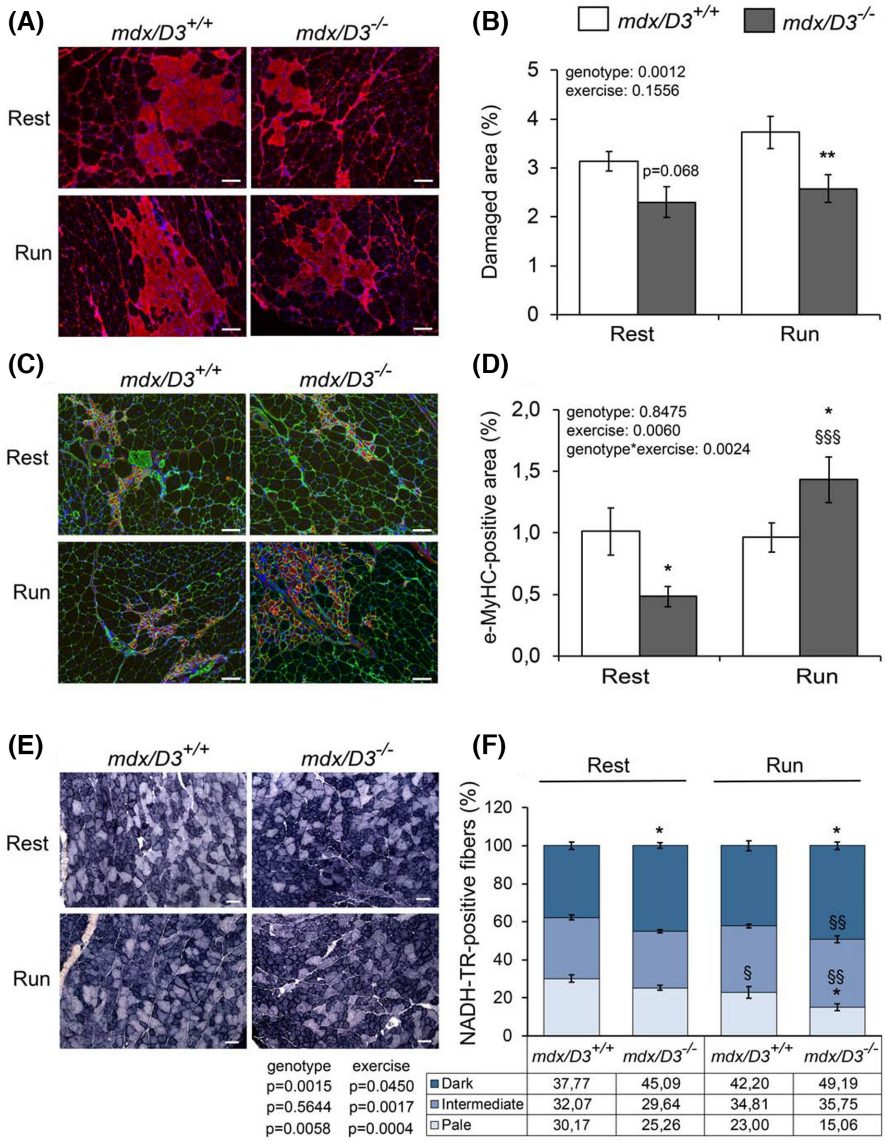

FIGURE 8 *mdx/D3*$^{-/-}$ mice display reduced muscle damage, improved regeneration, and enhanced oxidative metabolism after exercise. Immunofluorescence and histological analyses of gastrocnemius/plantaris muscle (GP) from 5-month-old *mdx/D3*$^{-/-}$ and *mdx/D3*$^{+/+}$ subjected to five weekly sessions of endurance exercise (Run) or sedentary (Rest). (A) Transverse sections of GP muscle stained with anti-IgG/IgM antibody (red) and counterstained with Hoechst. (B) Quantification of the necrotic areas in entire GP muscle sections. (C) GP transverse sections coimmunostained with anti-eMyHC (red), anti-laminin (green), and counterstained with Hoechst. (D) Quantification of the regenerating areas in entire GP muscle sections. The data in graphs shown in panels B and D are expressed as the percentage of the total GP cross-sectional area and are reported as means ± SEM (Run: $n = 8$ mice/group; Rest: $n = 7$ mice/group). Quantification was carried out in at least three sections per individual mouse. Statistical differences were assessed by two-way ANOVA analysis (p values of each variable effect are shown in graphs). (E) Representative NADH-TR staining on transversal sections of GP muscle. (F) Quantification of the number of differentially stained NADH-TR-positive fibers in fields of red GP muscle. The data in graph are expressed as the percentage in each category of the total number of fibers and are presented as means ± SEM ($n = 4$ mice/group). Quantification was carried out in two sections per individual mouse with at least 2000 fibers counted per section. Statistical differences were assessed by two-way ANOVA analysis (p values of each variable effect are shown next to the data table). Post hoc tests for multiple comparisons between groups were performed by Fisher's PLSD test. (*): *mdx/D3*$^{-/-}$ versus *mdx/D3*$^{+/+}$, *$p < .05$ and **$p < .01$; (§): Run versus Rest, $^{§}p < .05$, $^{§§}p < .01$, and $^{§§§}p < .001$. Scale bar: 100 μm.

myogenic progenitor cells, and the proper timing of injury-induced muscle regeneration.[31] In particular, during the early phase of regeneration induced by intramuscular injection of cardiotoxin, cyclin D3-null myogenic progenitors displayed a reduced rate of proliferation and an enhanced propensity to differentiate, whereas at later stages, regenerated cyclinD3-null myofibers appeared smaller in size compared to wild-type controls.[31] However, the muscle regeneration process appeared delayed, but not grossly defective, in the absence of cyclin D3.

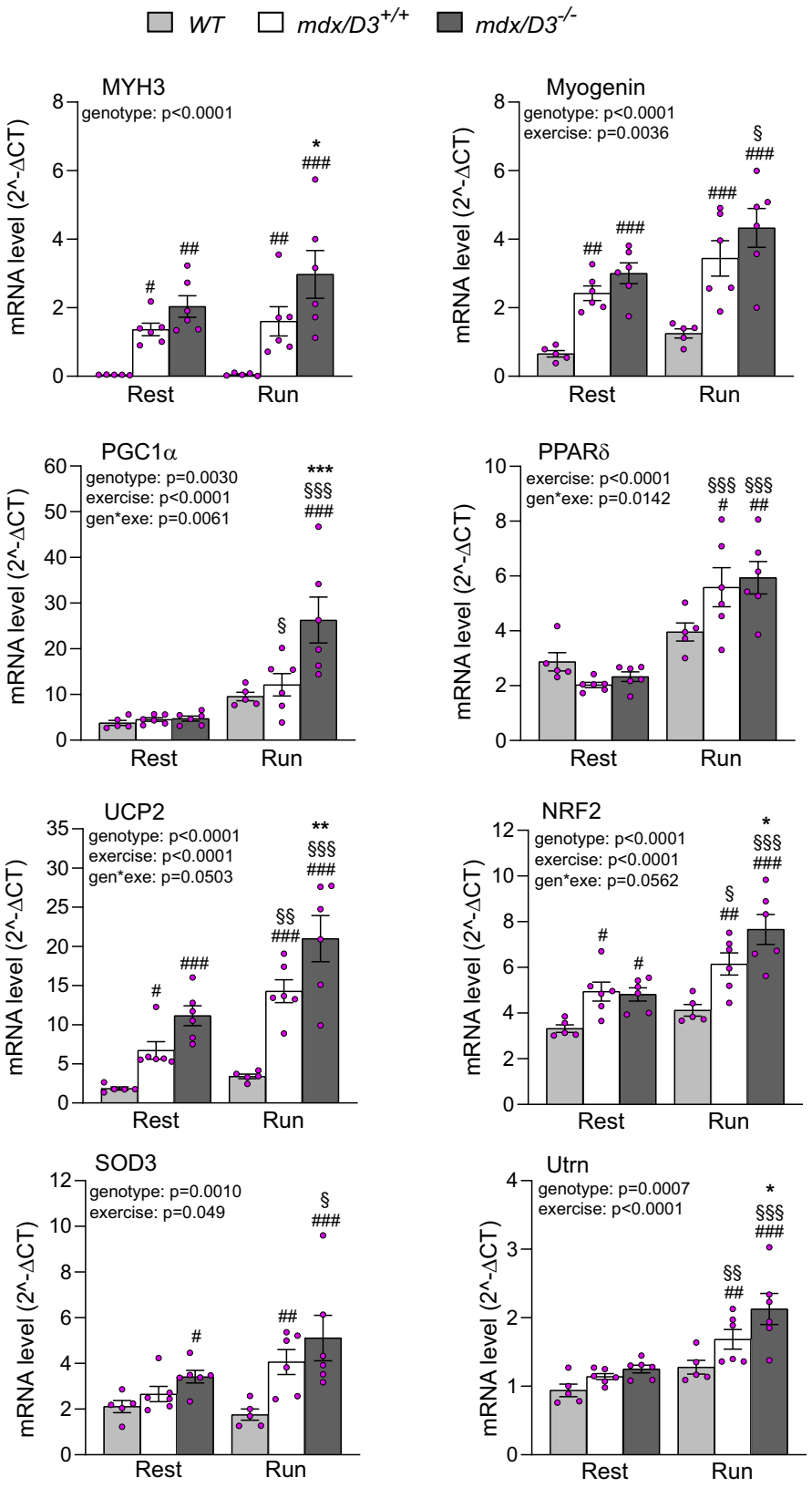

FIGURE 9 Gene expression analyses of muscles from sedentary and exercised mice. mRNA levels of the indicated genes were measured by real-time PCR in quadriceps muscles isolated from 5-month-old sedentary (Rest) and exercised (Run) *WT* (C57BL10), *mdx/D3*$^{-/-}$, and *mdx/D3*$^{+/+}$ mice. Expression data were normalized to TBP, used as endogenous control, and are reported as average 2^−ΔCT values ± SEM (*WT*: $n = 5$, *mdx/D3*$^{+/+}$: $n = 6$, and *mdx/D3*$^{-/-}$: $n = 6$). Statistical differences were assessed by two-way ANOVA analysis (p values of each variable effect are shown above graphs). Post hoc tests for multiple comparisons between groups were performed by Fisher's PLSD test (*$p < .05$, **$p < .01$, and ***$p < .001$ for *mdx/D3*$^{-/-}$ vs. *mdx/D3*$^{+/+}$; $^{§}p < .05$, $^{§§}p < .01$, and $^{§§§}p < .001$ for Run vs. Rest; $^{\#}p < .05$, $^{\#\#}p < .01$, and $^{\#\#\#}p < .001$ for *mdx/D3*$^{-/-}$ or *mdx/D3*$^{+/+}$ vs. *WT*).

A relevant finding from our study concerns the response of dystrophic mice lacking cyclin D3 to physical exercise, an experimental approach that is widely used to exacerbate disease severity to better model the muscle pathology seen in patients with DMD. Loss of cyclin D3 resulted in better performance of *mdx* mice in repeated trials of endurance exercise. Accordingly, force measurements conducted on TA muscles in situ indicated a significant reduction in force drop following repetitive electrical stimulations. The enhanced exercise tolerance and the

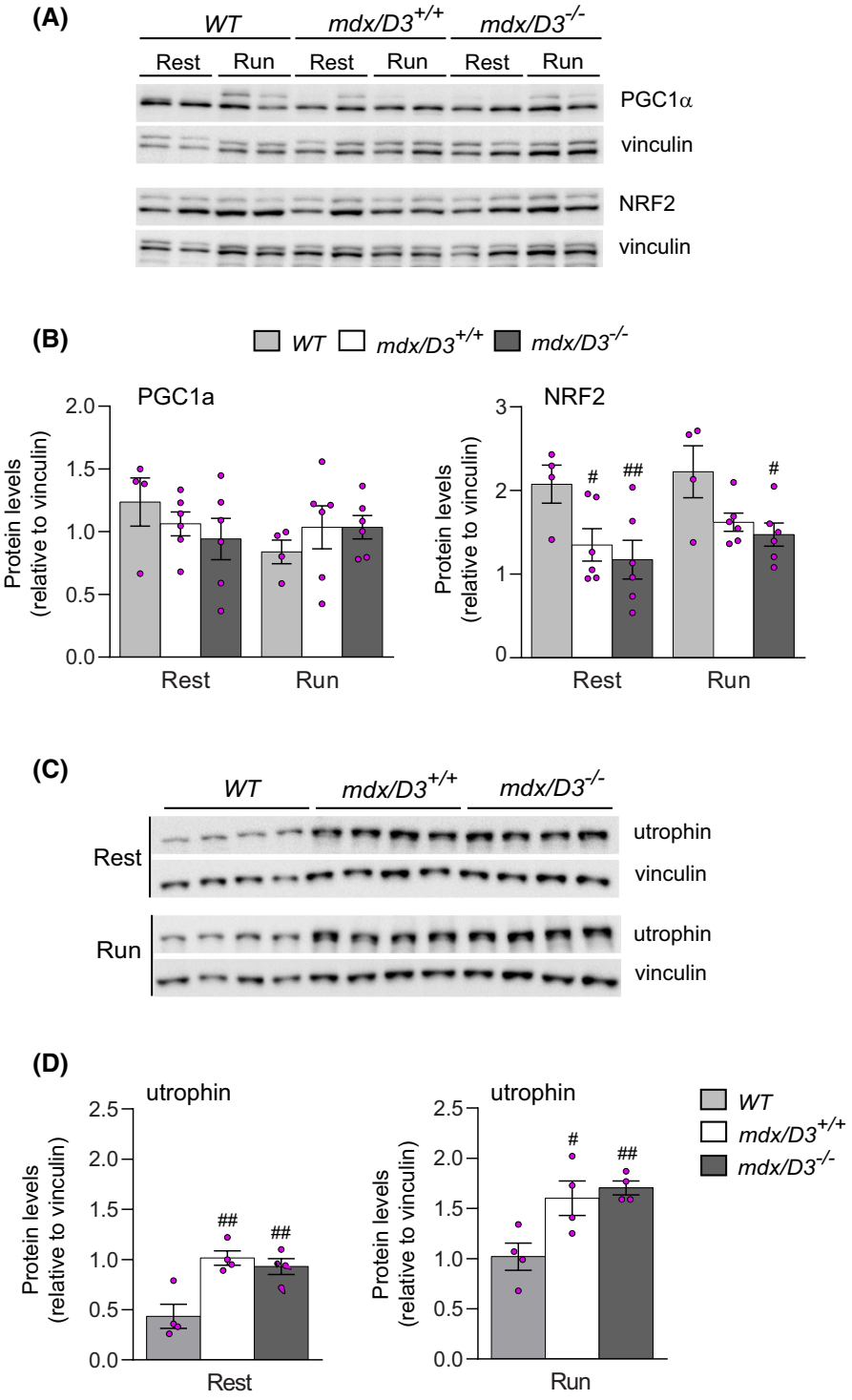

FIGURE 10 Protein expression analyses of muscles from sedentary and exercised mice. Expression levels of the indicated proteins were measured by Western blot of whole protein lysates of muscles isolated from 5-month-old sedentary (Rest) and exercised (Run) *WT* (C57BL10), *mdx/D3*$^{-/-}$, and *mdx/D3*$^{+/+}$ mice. (A) Representative Western blots for PGC1α, NRF2, and vinculin protein levels in gastrocnemius/plantaris muscle. (B) Densitometry analysis of band intensities. Quantitative values were computed as ratios of PGC1α to vinculin and NRF2 to vinculin and are reported as means ± SEM (*WT*: $n = 4$, *mdx/D3*$^{+/+}$: $n = 6$, and *mdx/D3*$^{-/-}$: $n = 6$). (C) Representative western blots for utrophin and vinculin protein levels in tibialis anterior muscle. (D) Quantitative analysis of band intensities by densitometry. Values were expressed as utrophin-to-vinculin ratios and are presented as means ± SEM ($n = 4$ mice/group). Statistical differences were assessed by two-way ANOVA analysis (PGC1α, effect of genotype: $p = .8948$, and effect of exercise: $p = .3562$; NRF2, effect of genotype: $p = .0016$, and effect of exercise: $p = .1562$) or one-way ANOVA analysis (utrophin Rest: $p = .0034$; utrophin Run: $p = .0111$). (#) Indicates statistical analysis by Fisher's PLSD post hoc test in the comparisons of *mdx/D3*$^{-/-}$ or *mdx/D3*$^{+/+}$ versus *WT* ($^{\#}p < .05$, $^{\#\#}p < .01$).

reduced muscle fatigability after in-situ stimulation observed in *mdx/D3*$^{-/-}$ mice correlate well with the slower, more oxidative profile of their muscle fibers and concur to suggest that the absence of cyclin D3 may protect dystrophic muscle from mechanical damage and fatigability. It should be emphasized, however, that the endurance exercise capacity of an organism relies largely on muscle oxidative capacity, but is also influenced by several additional variables, such as, for example, cardiac and pulmonary function. Since *mdx/D3*$^{-/-}$ mice lack cyclin D3 in the germinal line, we cannot exclude the possible contribution of tissues other than skeletal muscle to the observed improvement in exercise performance.

Remarkably, immunohistochemical analysis of GP muscle after the last bout of exercise revealed shifts from glycolytic toward more oxidative muscle fibers that were significantly more pronounced in *mdx* mice lacking cyclin D3. Furthermore, GP muscles from exercised *mdx/*

D3$^{-/-}$ mice appeared less damaged than *mdx* control muscles, and most importantly, we observed a regenerative burst following endurance exercises in *mdx/D3*$^{-/-}$ muscle but not in control *mdx/D3*$^{+/+}$ muscle. These findings suggest that the slowdown in the degeneration/regeneration circuit, observed in *mdx/D3*$^{-/-}$ mice during the initial phases of the disease, may preserve the regenerative potential of muscle by preventing the rapid exhaustion of satellite cells and by maintaining a more favorable environment for muscle precursor cell activation and differentiation when the muscle is exposed to contraction-induced injury during exercise.

Gene expression analyses performed in quadriceps muscles not only confirmed an enhancement of regeneration in exercised *mdx/D3*$^{-/-}$ versus *mdx/D3*$^{+/+}$ mice but also highlighted increased mRNA levels of utrophin and a number of genes involved in oxidative metabolism and response to oxidative stress, such as PGC1α, UCP2, and NRF2.

However, no significant changes were observed in the steady-state protein levels of PGC1α, NRF2, or utrophin in GP or TA muscles of exercised *mdx/D3*$^{-/-}$ mice compared with the corresponding *mdx/D3*$^{+/+}$ controls. Although we cannot exclude the different susceptibility of different muscle groups to the applied exercise challenge, the observed discrepancy between mRNA and protein levels might be explained by the time of muscle tissue collection after the last bout of exercise (2–4 h). In fact, mRNA transcripts encoding metabolic genes are typically found transiently increased at 4–8 h after an exercise bout, returning to basal levels within 24 h, whereas alteration of the corresponding protein levels is a function of their half-lives. Usually, proteins display a modest increase at 18–24 h post-exercise and gradually attain higher steady-state levels in response to pulsed increases in relative mRNA expression during frequently repeated exercise bouts.[60,61] The running protocol used in this study, with weekly repeated exercise sessions, was planned to periodically accelerate muscle damage rather than to study long-term muscle adaptation to exercise training, which would require more frequently repeated exercise bouts.

In skeletal muscle, an orchestrated network of signaling pathways is involved in response to increased contractile activity, such as Ca^{2+}-dependent, AMPK, and p38/MAPK pathways.[47] These signaling pathways converge on activation of MEF2 and NFAT, pivotal transcription factors involved in transcriptional regulation of oxidative metabolism and slow myofiber-specific genes, including PGC1a[62–64] and utrophin.[55,65] Our previous studies[19] and results reported here indicate that cyclin D3 deficiency can stimulate the transcriptional activity of MEF2 and NFAT and activation of AMPK in non-dystrophic muscle. Furthermore, there is evidence that MEF2D, NFATC3, and PGC1α are specifically targeted for phosphorylation by cyclinD3-CDK6 complexes.[22] Thus, we surmise that cyclin D3 depletion and exercise may cooperatively activate MEF2, NFAT, and AMPK, which might explain the observed enhancement of exercise-mediated mRNA induction of oxidative metabolism and oxidative stress-responsive genes in dystrophic muscle lacking cyclin D3.

In conclusion, our study indicates that cyclin D3 genetic inactivation in the *mdx* mouse model of DMD can ameliorate several histopathological signs of the disease, and this appears to be largely due to the promotion of a slower, more oxidative skeletal muscle phenotype. These findings suggest that an inhibition of cyclin D3 expression or activity may be a therapeutic strategy to treat DMD. However, the mouse model used in the present study lacks cyclin D3 in the germinal line and this influences the skeletal muscle phenotype before manifestation of the first symptoms of disease. Therefore, in light of a possible translational approach, further studies are needed to assess whether pharmacologic or gene therapy-mediated knockdown of cyclin D3 in *mdx* mice would lead to beneficial effects when the signs of the disease are already evident.

AUTHOR CONTRIBUTIONS

Agnese Bonato designed and performed histological, immunohistochemical, and molecular biology analyses and analyzed and interpreted the data; Giada Raparelli contributed to performing and analyzing histological and immunofluorescence analyses; Siro Luvisetto designed, performed, and analyzed the treadmill running experiments; Flavia Forconi performed the in-situ functional experiments and analyzed data; Marianna Cosentino analyzed the in-situ functional data; Felice Tirone discussed results and performed statistical analyses; Emanuele Rizzuto supervised the in-situ functional experiments, analyzed and interpreted the data, participated in scientific discussion, and reviewed the paper; Maurizia Caruso conceived the project, supervised the study, interpreted the data, and wrote the paper. All authors have read and approved the final manuscript.

ACKNOWLEDGMENTS

We thank Prof. Piotr Sicinski (Dana Farber Cancer Institute, Boston, MA, USA) for kindly providing cyclin D3 knockout mice, Prof. Antonio Musarò (DAHFMO-Unit of Histology and Medical Embryology, Sapienza University of Rome) for helpful discussions, and Carmine Nicoletti for the technical support. Thanks are also due to Francesca De Santa, Alessio Torcinaro, Luca Madaro, and Lucia Latella for donating useful reagents. This work was supported by funding from Duchenne Parent Project, The Netherlands, DPP_NL (grant # 19.018) to M. Caruso. M. Cosentino holds a fellowship from IBSA Foundation for Scientific Research.

DISCLOSURES

The authors declare that they have no conflict of interest.

DATA AVAILABILITY STATEMENT

Data that support the findings of this study are available in this article.

ORCID

Maurizia Caruso https://orcid.org/0000-0001-5445-6343

REFERENCES

1. Flanigan KM. Duchenne and Becker muscular dystrophies. *Neurol Clin*. 2014;32:671-688.
2. Heydemann A. Skeletal muscle metabolism in Duchenne and Becker muscular dystrophy—implications for therapies. *Nutrients*. 2018;10:796-820.
3. Mendell JR, Rodino-Klapac L, Sahenk Z, et al. Gene therapy for muscular dystrophy: lessons learned and path forward. *Neurosci Lett*. 2012;527:90-99.
4. Berardi E, Annibali D, Cassano M, Crippa S, Sampaolesi M. Molecular and cell-based therapies for muscle degenerations: a road under construction. *Front Physiol*. 2014;5:119.
5. Guiraud S, Davies KE. Pharmacological advances for treatment in Duchenne muscular dystrophy. *Curr Opin Pharmacol*. 2017;34:36-48.
6. Yao S, Chen Z, Yu Y, et al. Current pharmacological strategies for Duchenne muscular dystrophy. *Front Cell Dev Biol*. 2021;9:689533.
7. Schiaffino S, Reggiani C. Fiber types in mammalian skeletal muscles. *Physiol Rev*. 2011;91:1447-1531.
8. Webster C, Silberstein L, Hays AP, Blau HM. Fast muscle fibers are preferentially affected in Duchenne muscular dystrophy. *Cell*. 1988;52:503-513.
9. Moens P, Baatsen PH, Maréchal G. Increased susceptibility of EDL muscles from mdx mice to damage induced by contractions with stretch. *J Muscle Res Cell Motil*. 1993;14:446-451.
10. Ljubicic V, Matthew B, Jasmin BJ. The therapeutic potential of skeletal muscle plasticity in Duchenne muscular dystrophy: phenotypic modifiers as pharmacologic targets. *FASEB J*. 2014;28:548-568.
11. Chakkalakal JV, Harrison MA, Carbonetto S, Chin E, Michel RN, Jasmin BJ. Stimulation of calcineurin signaling attenuates the dystrophic pathology in mdx mice. *Hum Mol Genet*. 2004;13:79-388.
12. Stupka N, Plant DR, Schertzer JD, et al. Activated calcineurin ameliorates contraction-induced injury to skeletal muscles of mdx dystrophic mice. *J Physiol*. 2006;575:2645-2656.
13. Chalkiadaki A, Igarashi M, Nasamu AS, Knezevic J, Guarente L. Muscle-specific SIRT1 gain-of-function increases slow- twitch fibers and ameliorates pathophysiology in a mouse model of Duchenne muscular dystrophy. *PLoS Genet*. 2014;10:e1004490.
14. Ljubicic V, Miura P, Burt M, et al. Chronic AMPK activation evokes the slow, oxidative myogenic program and triggers beneficial adaptations in mdx mouse skeletal muscle. *Hum Mol Genet*. 2011;20:3478-3493.
15. Miura P, Chakkalakal JV, Boudreault L, et al. Pharmacological activation of PPARbeta/delta stimulates utrophin A expression in skeletal muscle fibers and restores sarcolemmal integrity in mature mdx mice. *Hum Mol Genet*. 2009;18:4640-4649.
16. Handschin C, Kobayashi YM, Chin S, Seale P, Campbell KP, Spiegelman BM. PGC-1alpha regulates the neuromuscular junction program and ameliorates Duchenne muscular dystrophy. *Genes Dev*. 2007;21:770-783.
17. Blanchet E, Annicotte JS, Pradelli LA, et al. E2F transcription factor-1 deficiency reduces pathophysiology in the mouse model of Duchenne muscular dystrophy through increased muscle oxidative metabolism. *Hum Mol Genet*. 2012;21:3910-3917.
18. Rossi G, Bonfanti C, Antonini S, et al. Silencing Nfix rescues muscular dystrophy by delaying muscle regeneration. *Nat Commun*. 2017;8:1055.
19. Giannattasio S, Giacovazzo G, Bonato A, et al. Lack of cyclin D3 induces skeletal muscle fiber-type shifting, increased endurance performance and hypermetabolism. *Sci Rep*. 2018;8:12792.
20. Sherr CJ. D-type cyclins. *Trends Biochem Sci*. 1995;20:187-190.
21. Dick FA, Rubin SM. Molecular mechanisms underlying RB protein function. *Nat Rev Mol Cell Biol*. 2013;14:297-306.
22. Anders L, Ke N, Hydbring P, et al. A systematic screen for CDK4/6 substrates links FOXM1 phosphorylation to senescence suppression in cancer cells. *Cancer Cell*. 2011;20:620-634.
23. Hydbring P, Malumbres M, Sicinski P. Non-canonical functions of cell cycle cyclins and cyclin-dependent kinases. *Nat Rev Mol Cell Biol*. 2016;17:280-292.
24. Fajas L. Re-thinking cell cycle regulators: the cross-talk with metabolism. Front. *Oncol*. 2013;3:4.
25. Fantl V, Edwards PA, Steel JH, Vonderhaar BK, Dickson C. Mice lacking cyclin D1 are small and show defects in eye and mammary gland development. *Genes Dev*. 1995;9:2364-2372.
26. Sicinski P, Donaher JL, Parker SB, et al. Cyclin D1 provides a link between development and oncogenesis in the retina and breast. *Cell*. 1995;82:621-630.
27. Sicinski P, Donaher JL, Geng Y, et al. Cyclin D2 is an FSH-responsive gene involved in gonadal cell proliferation and oncogenesis. *Nature*. 1996;384:470-474.
28. Sicinska E, Aifantis I, Le Cam L, et al. Requirement for cyclin D3 in lymphocyte development and T cell leukemias. *Cancer Cell*. 2003;4:451-461.
29. Ciemerych MA, Kenney AM, Sicinska E, et al. Development of mice expressing a single D-type cyclin. *Genes Dev*. 2002;16:3277-3289.
30. Bartkova J, Lukas J, Strauss M, Bartek J. Cyclin D3: requirement for G1/S transition and high abundance in quiescent tissues suggest a dual role in proliferation and differentiation. *Oncogene*. 1998;17:1027-1037.
31. De Luca G, Ferretti R, Bruschi M, Mezzaroma E, Caruso M. Cyclin D3 critically regulates the balance between self-renewal and differentiation in skeletal muscle stem cells. *Stem Cells*. 2013;31:2478-2491.
32. Tseng BS, Zhao P, Pattison JS, et al. Regenerated mdx mouse skeletal muscle shows differential mRNA expression. *J Appl Physiol*. 2002;93:537-545.
33. Strimpakos G, Corbi N, Pisani C, et al. Novel adeno-associated viral vector delivering the utrophin gene regulator jazz counteracts dystrophic pathology in mdx mice. *J Cell Physiol*. 2014;229:1283-1291.
34. Rizzuto E, Pisu S, Musarò A, Del Prete Z. Measuring neuromuscular junction functionality in the SOD1(G93A)

animal model of amyotrophic lateral sclerosis. *Ann Biomed Eng*. 2015;43:2196-2206.
35. Forconi F, Apa L, Pisu S, et al. Development of a novel technique for the measurement of neuromuscular junction functionality in isotonic conditions. *Cell Mol Bioeng*. 2022;15:255-265.
36. Brooks SV, Faulkner JA. Contractile properties of skeletal muscles from young, adult and aged mice. *J Physiol*. 1988;404:71-82.
37. Pelosi L, Berardinelli MG, Forcina L, et al. Increased levels of interleukin-6 exacerbate the dystrophic phenotype in mdx mice. *EBioMedicine*. 2015;2:285-293.
38. Sharp PS, Bye-a-Jee H, Wells DJ. Physiological characterization of muscle strength with variable levels of dystrophin restoration in mdx mice following local antisense therapy. *Mol Ther*. 2011;19:165-171.
39. Briguet A, Courdier-Fruh I, Foster M, Meier T, Magyar JP. Histological parameters for the quantitative assessment of muscular dystrophy in the mdx-mouse. *Neuromuscul Disord*. 2004;14:675-682.
40. Laghi V, Ricci V, De Santa F, Torcinaro A. A user-friendly approach for routine histopathological and morphometric analysis of skeletal muscle using CellProfiler software. *Diagnostics (Basel)*. 2022;12:561.
41. Blaauw B, Schiaffino S, Reggiani C. Mechanisms modulating skeletal muscle phenotype. *Compr Physiol*. 2013;3:1645-1687.
42. Allen DL, Harrison BC, Maass A, Bell ML, Byrnes WC, Leinwand LA. Cardiac and skeletal muscle adaptations to voluntary wheel running in the mouse. *J Appl Physiol*. 2001;90:1900-1908.
43. Egan DF, Shackelford DB, Mihaylova MM, et al. Phosphorylation of ULK1 (hATG1) by AMP-activated protein kinase connects energy sensing to mitophagy. *Science*. 2011;331:456-461.
44. Bodine SC, Latres E, Baumhueter S, et al. Identification of ubiquitin ligases required for skeletal muscle atrophy. *Science*. 2001;294:1704-1708.
45. Gomes MD, Lecker SH, Jagoe RT, Navon A, Goldberg AL. Atrogin-1, a muscle-specific F-box protein highly expressed during muscle atrophy. Proc Natl Acad Sci USA 2001; 98: 14440–14445.
46. Herzig S, Shaw RJ. AMPK: guardian of metabolism and mitochondrial homeostasis. *Nat Rev Mol Cell Biol*. 2018;19:121-135.
47. Lira VA, Benton CR, Yan Z, Bonen A. PGC-1alpha regulation by exercise training and its influences on muscle function and insulin sensitivity. *Am J Physiol Endocrinol Metab*. 2010;299:E145-E161.
48. Fan W, Waizenegger W, Lin CS, et al. PPARδ promotes running endurance by preserving glucose. *Cell Metab*. 2017;25:1186-1193.
49. Kitaoka Y. The role of Nrf2 in skeletal muscle on exercise capacity. *Antioxidants*. 2021;10:1712.
50. Bo H, Jiang N, Ma G, et al. Regulation of mitochondrial uncoupling respiration during exercise in rat heart: role of reactive oxygen species (ROS) and uncoupling protein 2. *Free Radic Biol Med*. 2008;44:1373-1381.
51. Yan Z, Spaulding HR. Extracellular superoxide dismutase, a molecular transducer of health benefits of exercise. *Redox Biol*. 2020;32:101508.
52. Rius-Pérez S, Torres-Cuevas I, Millán I, Ortega ÁL, Pérez S. PGC-1α, inflammation, and oxidative stress: an integrative view in metabolism. *Oxid Med Cell Longev*. 2020;2020:1452696.
53. Mailloux RJ, Harper ME. Uncoupling proteins and the control of mitochondrial reactive oxygen species production. *Free Radic Biol Med*. 2011;51:1106-1115.
54. Ma Q. Role of Nrf2 in oxidative stress and toxicity. *Annu Rev Pharmacol Toxicol*. 2013;53:401-426.
55. Chakkalakal JV, Stocksley MA, Harrison MA, Angus LM, Deschenes-Furry J, St-Pierre S, Megeney LA, Chin ER, Michel RN, Jasmin BJ. Expression of utrophin a mRNA correlates with the oxidative capacity of skeletal muscle fiber types and is regulated by calcineurin/NFAT signaling. Proc Natl Acad Sci USA 2003; 100:7791–7796.
56. Garcia D, Shaw RJ. AMPK: mechanisms of cellular energy sensing and restoration of metabolic balance. *Mol Cell*. 2017;66:789-800.
57. Lopez-Mejia IC, Lagarrigue S, Giralt A, et al. CDK4 phosphorylates AMPKα2 to inhibit its activity and repress fatty acid oxidation. *Mol Cell*. 2017;68:336-349.
58. Sacco A, Mourkioti F, Tran R, et al. Short telomeres and stem cell exhaustion model Duchenne muscular dystrophy in mdx/mTR mice. *Cell*. 2010;143:1059-1071.
59. Chang NC, Chevalier FP, Rudnicki MA. Satellite cells in muscular dystrophy—lost in polarity. *Trends Mol Med*. 2016;22:479-496.
60. Perry CG, Lally J, Holloway GP, Heigenhauser GJ, Bonen A, Spriet LL. Repeated transient mRNA bursts precede increases in transcriptional and mitochondrial proteins during training in human skeletal muscle. *J Physiol*. 2010;588:4795-4810.
61. Hawley JA, Hargreaves M, Joyner MJ, Zierath JR. Integrative biology of exercise. *Cell*. 2014;159:738-749.
62. Lin J, Wu H, Tarr PT, et al. Transcriptional co-activator PGC-1 alpha drives the formation of slow-twitch muscle fibres. *Nature*. 2002;418:797-801.
63. Handschin C, Rhee J, Lin J, Tarr PT, Spiegelman BM. An autoregulatory loop controls peroxisome proliferator-activated receptor gamma coactivator 1alpha expression in muscle. Proc Natl Acad Sci USA 2003; 100: 7111–7116.
64. Czubryt MP, McAnally J, Fishman GI, Olson EN. Regulation of peroxisome proliferator activated receptor gamma coactivator 1 alpha (PGC-1 alpha) and mitochondrial function by MEF2 and HDAC5. Proc Natl Acad Sci USA 2003; 100: 1711–1716.
65. Angus LM, Chakkalakal JV, Méjat A, et al. Calcineurin-NFAT signaling, together with GABP and peroxisome PGC-1{alpha}, drives utrophin gene expression at the neuromuscular junction. *Am J Physiol Cell Physiol*. 2005;289:C908-C917.

SUPPORTING INFORMATION

Additional supporting information can be found online in the Supporting Information section at the end of this article.

How to cite this article: Bonato A, Raparelli G, Luvisetto S, et al. Cyclin D3 deficiency promotes a slower, more oxidative skeletal muscle phenotype and ameliorates pathophysiology in the *mdx* mouse model of Duchenne muscular dystrophy. *The FASEB Journal*. 2023;37:e23025. doi:10.1096/fj.202201769R